Hotspots, refuges, and rising risk: mapping tropical hunting pressure across space and time

Martin Philippe-Lesaffre[1,*], Iago Ferreiro-Arias[1,2], Jedediah F. Brodie[3,4,5], Dominik Schüßler[6], Laura Maeso-Pueyo[1], Ana Benítez-López[1]

[1] Department of Biogeography and Global Change, Museo Nacional de Ciencias Naturales (MNCN-CSIC), Madrid, Spain

[2] Department of Conservation Biology and Global Change, Estación Biológica de Doñana (EBD-CSIC), Sevilla, Spain

[3] Division of Biological Sciences, University of Montana, Missoula, MT 59812, USA

[4] Wildlife Biology Program, University of Montana, Missoula, MT 59812, USA

[5] Institute of Biodiversity and Environmental Conservation, Universiti Malaysia Sarawak, 94300 Kota Samarahan, Malaysia

[6] Institute of Biology and Chemistry, University of Hildesheim, Hildesheim, Germany

*Corresponding author: Martin Philippe-Lesaffre (martin.philippe@mncn.csic.es)

Abstract

Hunting is a major driver of global extinctions, yet the spatial footprint and temporal trend of this pressure is lacking at global scale, limiting our ability to achieve international policy targets. Here, we present the first standardized global maps of hunting pressure across the tropics, based on a machine learning algorithm trained on 2,463 hunted and non-hunted tropical sites, spatially and temporally matched to ecological and socio-economic predictors. We estimate that the spatial footprint of hunting pressure extends over 29 mill. km^2 of tropical forests, with distinct hotspots of high hunting pressure in the Indomalayan realm (e.g., China, Sri Lanka, Western India), the Atlantic Forest, and parts of West Africa. Refuges of low hunting pressure persist in remote areas of interior Borneo, Papua New Guinea, Central Africa, and the western Amazon. Enhanced human accessibility has facilitated the spread of hunting pressure between 2000-2015, most notably in traditionally considered undisturbed remote regions like the Amazon basin, as well as in areas already facing high pressure such as China and Indonesia. Spatio-temporal dynamics varied among realms: the Indomalayan region experienced marked increases in hunting within existing hotspots, the Neotropics exhibited no clear temporal trends, and the Afrotropical realm remained relatively stable. Our standardized spatio-temporal assessment provides a blueprint to inform conservation priorities, allowing for targeted management actions and informed policy interventions to mitigate hunting impacts. Our pan-tropical maps of hunting pressure can also contribute to integrated assessments of multiple threats to biodiversity at broad scales, facilitating the monitoring of progress towards international policy targets.

Main Text

Introduction

From agoutis and songbirds to hornbills and rhinos, humans have hunted wildlife for millennia. Nowadays, however, unsustainable hunting for consumption and trade of wild animals represents a major extinction threat to terrestrial vertebrates (1–3). Wild vertebrates are harvested for a variety of reasons, both legally and illegally. These include direct consumption as food (4), the production of traditional medicine, tools, ornaments, as well as for the pet trade, particularly with birds (5, 6). Hunting impacts thousands of bird and mammal species globally, especially for trading purpose (6), leading to significant declines for some species (7) and acting as a primary driver of extinction (6, 8). Additionally, vertebrate species are non-randomly harvested, with specific traits such as body size, colorful plumage, or body parts with ornamental uses, making them more likely targeted than others (6, 9–12), leading to increased endangerment of phylogenetically clustered branches of the tree of life (6).

Data on the extent, patterns, and trends of hunting pressure are crucial for guiding global and national conservation and sustainable development priorities. Unlike most other anthropogenic threats such as logging, urbanization, agriculture, and fire events (13–15), which can be effectively monitored through remote sensing (16, 17), hunting remains challenging to be detected, due to its cryptic and often clandestine nature. Consequently, hunting represents only a small fraction (approximately 5%) of the available datasets on global threats (18). Furthermore, the cryptic impacts of hunting contribute to the phenomenon of 'empty forests' (19) or 'half-empty forests' (20), terms that describe ecosystems that appear structurally intact but have experienced significant wildlife declines due to unsustainable harvesting (21).

Accurate estimates of the magnitude and spatial extent of hunting pressure in tropical regions at fine spatial resolutions require innovative approaches that are spatially explicit and do not solely rely on remote sensing. To address this need, several methods have been developed, including mechanistic and correlative models to predict hunting pressure (3), biomass offtake (22), hunting-induced abundance declines (23, 24). Alternative approaches map the probability of species being threatened by hunting within grid cells, based on IUCN species' geographic ranges and qualitative data from threat assessments (25). Collectively, these methodologies have significantly advanced global mapping efforts, enhancing our understanding of the spatial footprint of hunting impacts across the tropics. Yet, the existing approaches have several shortcomings that hamper our ability to fully gauge the pervasiveness and intensity of hunting pressure across the globe, as well as its implementation in

cumulative threat maps or to inform international policy processes. For example, mechanistic models produce a unitless hunting pressure index that lacks external validation and calibration, limiting their practical use. In turn, correlative models are limited by the low availability of abundance data and the often-unbalanced spatial coverage of empirical studies. Additionally, because these models depend on species distributions, their resulting maps cannot be easily integrated with other human pressure layers (e.g., Anthromes, Global Human Modification, Human Footprint, Low Impact Areas; (26)). Finally, pressure maps based on the distribution of species threatened by hunting (e.g., (25, 27)) suffer from known limitations inherent to the IUCN assessment process (28, 29). These include inconsistent evaluation criteria among species, low spatial accuracy at finer scales, and reliance on generalized range-wide assessments rather than spatially explicit threat quantification, thus inadequately capturing local variability in hunting pressures (e.g., (30)).

To address these limitations, we compiled an extensive geo-referenced dataset consisting of 2,463 hunted and non-hunted sites across tropical regions. Each site was precisely matched, both spatially and temporally, with a set of socio-economic and ecological predictors commonly recognized as major drivers of hunting at large spatial scales (Table 1). Utilizing these spatially and temporally aligned datasets, we trained supervised binary classifiers using random forests to predict the probability of hunting occurrence across different time periods. The resulting hunting pressure (HP), expressed as a standardized probability score ranging from 0 to 1, facilitating integration with other human pressure layers while being able to capture spatial variation in HP at fine resolution. Specifically, we focused our analyses on the years 2000 and 2015, periods for which predictor layers were available. This temporal framework, already applied for forest fragmentation (31), provides an important methodological advancement by enabling the identification of both global, regional and local trends in HP. Our spatially and temporally explicit maps highlight regions experiencing low or high HP, as well as areas where hunting has increased or decreased between 2000-2015. This provides a robust, standardized, and spatially explicit framework to effectively target conservation interventions at regional, national, and subnational scales.

Results

Hunting pressure model

The random forests used to predict hunting pressure (HP) across tropical regions for the years 2000 and 2015 demonstrated strong predictive performance, with an area under the receiver operating curve (AUC) of 0.90 ± 0.016, a Matthew correlation coefficient (MCC) of 0.58 ± 0.031 and an accuracy of 0.81 ± 0.016 (mean ± standard deviation; see *SI Appendix*, Fig. *S1* to Fig. *S5*). Our model identified

distance to the nearest human settlement as the most important predictor (mean absolute Shapley additive explanations - mean(|SHAP|) = 0.085 ± 0.064; *SI Appendix*, Fig. *S6*). Marginal effects indicated that HP increased notably within a 25 km radius around settlements, increasing linearly as distance decreases (*SI Appendix*, Fig. *S7*). The proportion of forest cover within a 20 km buffer was the second most important predictor (mean(|SHAP|) = 0.057 ± 0.035), with HP peaking at intermediate forest cover (~75%) and decreasing at both lower and higher extremes (*SI Appendix*, Fig. *S6* and Fig. *S7*). The Human Development Index (HDI) ranked third in importance (mean(|SHAP|) = 0.053 ± 0.042), with both low and high HDI values associated with elevated HP, suggesting a non-linear relationship. Livestock biomass and net primary productivity showed moderate importance, with higher HP in areas with moderately low livestock density (but not the lowest) and in highly productive forests (*SI Appendix*, Fig. *S6* and Fig. *S7*). All other predictors had comparatively limited contributions to model performance.

Spatial patterns of hunting pressure

HP in 2015 exhibited pronounced spatial heterogeneity across tropical regions (mean HP = 0.70 ± 0.16; Fig. 1). Most of the pantropical zone displayed an HP > 0.5 (~88% of the grid cells), with few remnants of low pressure (HP < 0.5, ~11% of the grid cells), and distinct, extensive hotspots of high pressure (HP > 0.9, ~9% of the grid cells). The Indomalayan realm contained the biggest and most intensively hunted hotspots, especially in China, Sri Lanka, Western Ghats (India), Peninsular Malaysia, and Sumatra, and Java (Indonesia). Additional hotspots were observed in West Africa (Afrotropical realm) and in the Atlantic Forest, Caribbean islands, southern Mexico and Guatemala (Neotropical realm). Refuge areas were primarily located in interior Borneo and Papua New Guinea (Indomalayan realm), Central Africa (Afrotropical realm), and the western Amazon Basin (Neotropical realm). Outside of these hotspots and refuges, HP was generally moderate but highly variable at local scales. Realm-level comparisons showed the Indomalayan region had the highest average HP (0.77 ± 0.15), followed by the Afrotropical (0.71 ± 0.13) and Neotropical (0.65 ± 0.13) realms (Bonferroni-corrected $p < 0.001$ for all comparisons; Fig. 2). Additionally, the Indomalayan realm had the highest proportion of hunting hotspots covering 25% of grid cells, and the lowest proportion of low HP areas (~6%). In contrast, both the Afrotropical and Neotropical realms had only ~4% of grid cells classified as hotspots, but low HP was more widespread in the Neotropics (~17%) compared to the Afrotropics (~8%).

At the country level, HP varied most widely in the Neotropical realm (0.50–0.88), followed by the Afrotropical (0.51–0.83), and Indomalayan realms (0.60–0.88) (Fig. 2, *SI Appendix*, Fig. *S8*). Countries with the highest average HP included Sri Lanka (0.88 ± 0.093), Jamaica (0.88 ± 0.093), China (0.85 ± 0.13), and Thailand (0.84 ± 0.11). In contrast, Guyana (0.50 ± 0.12), Namibia (0.51 ± 0.055), and

Somalia (0.54 ± 0.064) had the lowest values but also a very small area of tropical forest for the two African countries (*SI Appendix*, Fig. *S8*).

At the ecoregion level, trends differed slightly. The Neotropical realm again showed the highest variability in HP (0.47–0.93), followed closely by the Indomalayan (0.50–0.93), and then the Afrotropical realm (0.52–0.86) (SI Appendix, Fig. *S9*). Ecoregions characterized by high HP included the Northwestern Ghats montane forests and Malabar Coast moist forests (Western India), Puerto Rican dry and moist forests, and the Chao Phraya freshwater swamp forests (Central Thailand). In contrast, ecoregions with low HP were found in remote tropical areas such as the Solimões-Japurá, Juruá-Purus, and Uatumã-Trombetas moist forests in the Amazon Basin, the Northern New Guinea montane rainforests, and the Northern Triangle temperate forests in northern Myanmar (*SI Appendix*, Fig. *S9*).

Temporal changes in hunting pressure

Between 2000 and 2015, HP increased significantly across the tropics (mean change = 0.031 ± 0.083, $p < 0.001$*;* hereafter, all temporal changes refer to the absolute difference in HP between 2015 and 2000, i.e., HP2015 – HP2000). Most grid cells showed modest change, with only a few exhibiting substantial increases or decreases (minimum = –0.46; 20th percentile = –0.031; 40th = 0.0035; 60th = 0.040; 80th = 0.093; and maximum = 0.63, Fig. 3). Realm-level analysis indicated the greatest increase in the Indomalayan (0.046 ± 0.085) and the Neotropical realms (0.045 ± 0.087), while the Afrotropical realm experienced a slight but significant decrease (-0.0054 ± 0.058).

When analyzing spatial and temporal patterns together, the Indomalayan realm exhibited a positive linear relationship: areas with high HP in 2015 also experienced the largest increases since 2000, while low-pressure areas tended to show declines. This trend was consistent across spatial scales — including grid cell, country, and ecoregion levels. In contrast, the Neotropical and Afrotropical realms displayed more heterogeneous temporal dynamics, without a clear correlation between 2015 pressure and temporal change (Fig. 2; *SI Appendix*, Fig. *S10*, Fig. *S11* and Fig. *S12*).

At the national level, countries in the Indomalayan realm with the highest HP in 2015, such as China and Thailand, showed the most pronounced increases (change = 0.084 ± 0.079 and 0.078 ± 0.059, respectively). Conversely, Myanmar (-0.024 ± 0.061), Cambodia (-0.015 ± 0.080), Papua New Guinea (-0.012 ± 0.057), and Malaysia (-0.009 ± 0.062) were the only countries in the region to exhibit declining trends (*SI Appendix*, Fig. *S10* and Fig. *S13*). In the Neotropical realm, notable increases in HP were observed even in countries with initially low pressure, such as Venezuela and Colombia (change = 0.099 ± 0.086 and 0.084 ± 0.069, respectively). Declines were observed in Trinidad and Tobago (-0.031 ± 0.056), Cuba (-0.028 ± 0.063), and to a lesser extent, Guyana (-0.0061 ± 0.070) (*SI Appendix*, Fig. *S10* and Fig. *S13*). The Afrotropical realm remained comparatively stable over time, with most

countries experiencing minimal changes. Sixteen countries showed decreasing trends, including Namibia (-0.049 ± 0.064) and Somalia (-0.031 ± 0.040), both of which had low HP and slight declines (*SI Appendix*, Fig. *S10* and Fig. *S13*).

Ecoregional patterns matched national-level results. In the Indomalayan realm, temporal variability was highest and positively correlated with 2015 pressure. Five ecoregions experienced increases greater than 15%, including four in the Neotropics: Orinoco wetlands and Orinoco Delta swamp forests (eastern Venezuela and northern Guyana), Cordillera Central páramo (northern Peru and southern Ecuador), and Llanos (Colombia and Venezuela); and one in the Indomalayan realm: the Mentawai Islands rainforests (off the west coast of Sumatra) (*SI Appendix*, Fig. *S12* and Fig. *S14*). Unlike other ecoregions, the Mentawai Islands rainforests experienced a significant positive change but a relatively intermediate value of HP (0.65 ± 0.15) (*SI Appendix*, Fig. *S12* and Fig. *S14*). Only one ecoregion showed a decrease greater than 10%: the Irrawaddy freshwater swamp forests (coastal Myanmar, near the Bay of Bengal). No Neotropical or Afrotropical ecoregion exhibited increases above 10%, though several experienced decreases over 5%. These included the Central Andean dry puna (Andean Altiplano) and Tapajós–Xingu moist forests (eastern Amazon Basin) in the Neotropics, and the Highveld grasslands (South African inland plateau) in the Afrotropics (*SI Appendix*, Fig. *S12* and Fig. *S14*).

Discussion

A spatio-temporal index of hunting pressure

This study presents the first global assessment of hunting pressure (HP) across tropical forests using a standardized, non-species-specific index over time. Unlike previous approaches focused on species-level defaunation and extinction risk (23, 24), or on IUCN Red List threat assessments as spatial proxies for HP (25), our method directly estimates where hunting is likely to occur based on ecological and socio-economic drivers (see also (3)).Our approach unifies HP across motivations (e.g., subsistence and commercial), providing high-resolution global predictions based on observed hunted and non-hunted sites. In contrast to earlier efforts limited to specific realms (3) or regional studies (22, 32) this method provides a cohesive global perspective.

Our HP maps offer a major advance over previous proxy-based methods that rely on species' threat statuses (25) or general infrastructure proximity (17). These maps provide a single, intuitive metric of HP, making them easily integrable into cumulative threat assessments. This is especially valuable for identifying conservation priority areas, particularly for mammals and birds, which remain

disproportionately affected by hunting (8, 10). Furthermore, because our index is temporally explicit, it supports the growing need to integrate time-varying threats into conservation planning (31).

Ecological and socio-economic drivers of hunting pressure

Across all models, accessibility (i.e., distance to the nearest human settlement) emerged as the strongest and most consistent predictor of HP, confirming prior findings (23, 24, 30). This relationship was observed globally and within each tropical realm independently (*SI Appendix*, Fig. *S15* to Fig. *S21*). In all cases, HP increased with proximity to human settlements, with increases beginning at ~25 km and peaking closest to settlements.

Forest characteristics also played important roles: Large, less-disturbed forest patches near protected area boundaries showed higher predicted HP, supporting the idea that these zones function as wildlife reservoirs and their surrounding are prolific hunting grounds (30, 33).This aligns with recent evidence that species survival often drops rapidly just outside protected areas (33).Other socio-economic predictors, such as population density, GDP, and livestock biomass availability were aligned with theoretical expectations but contributed less to model performance. These results underscore the opportunistic nature of hunting, which tends to be concentrated in accessible forested landscapes that are not fully disturbed by human infrastructures but not completely remote either.

Spatial patterns

Our predicted spatial patterns of HP only partially resemble what has been observed in previous studies (Ziegler et al., 2016; Benítez-López et al., 2019; Bogoni et al., 2022; Ferreiro-Arias et al., 2024). Clear hotspots emerged in the Indomalayan realm, especially in China, Sri Lanka, Western India, Peninsular Malaysia, Sumatra, and Java, consistent with documented patterns of hunting-induced defaunation (23, 34). China has been historically recognized as an important destination for illegal wildlife trade, yet recent evidence points out that illegal hunting is widespread across the country, and it concentrates towards the east (35). In turn, wildlife in Sri Lanka has been subjected to hunting from ca. 45,000 years ago (36), and our results indicate that this pressure is now pervasive and intense across the island. Additional hotspots were identified in West Africa and across the Atlantic Forest and the Caribbean islands. In contrast, areas of low pressure (putative wildlife refuges) were concentrated in remote zones such as interior Borneo, Papua New Guinea, parts of Central Africa, and the western Amazon, reinforcing the role of remoteness and low accessibility in mitigating hunting intensity (2, 37).

Temporal trends

Our results indicate a small but significant global increase in HP from 2000 to 2015. Though the global average was low (~3%), spatial heterogeneity was substantial, with some regions experiencing large increases and others showing declines. Accessibility remained the dominant driver: areas where access expanded, especially near growing village networks, tended to show increased HP. This pattern overlaps with regions of low forest integrity, such as Java, Sumatra, or southeastern China (17), where anthropogenic impacts like fragmentation are already high, and where synergistic effects of both pressures could be detrimental for terrestrial wildlife (38–40). Moreover, regions dominated by 'village' anthromes (41) largely overlap with areas experiencing increasing HP in our mapping, while 'wildland' anthromes are mostly located in refuge zones. These patterns highlight the importance of understanding how accessibility evolves over time and particularly the global encroachment of the last remote areas of the planet that hold undisturbed animal communities and maintain ecological integrity (42).

Integration into cumulative threat mapping

The first target of the Kunming-Montreal Global Biodiversity Framework (KMGBF) calls for accurate global mapping of multiple threats to biodiversity. While metrics like the STAR score rely on species-specific threat information from IUCN assessments (43), these data are limited by taxonomic biases, lack of spatial precision, and inconsistencies across species (28, 29). By contrast, spatially explicit layers such as the Forest Landscape Integrity Index (FLII) (17) better reflect landscape-level pressures but do not accurately capture hunting, relying instead on indirect proxies. The HP maps developed in this study help fill this gap. As a standardized and non-species-specific metric, they can be directly integrated into cumulative threat assessments advancing Target 6 of the KMGBF by improving hunting risk coverage, and Target 1 by supporting comprehensive spatial prioritization of conservation actions based on combined anthropogenic pressures.

Limitations and Future Directions

Our use of a binary classification approach (i.e., hunted or non-hunted) limits our ability to differentiate between varying intensities of hunting. This simplification means that areas under low but persistent pressure are treated the same as those under severe exploitation. Future models should explore multi-class or continuous approaches to quantify hunting pressure levels, which would require well-defined and spatially adaptable thresholds. Developing separate models for different hunting purposes (e.g., subsistence or commercial hunting) should be a priority for future research, as these types of hunting impact species and regions differently (e.g., see the case of pangolins in (44)).

Importantly, our models estimate the likelihood of hunting occurrence without incorporating biodiversity data at each site. This was intentional: our goal was to isolate potential hunting pressure

based solely on ecological and socio-economic conditions. However, to better infer ecological impacts, future efforts should integrate biodiversity metrics, such as species richness or functional composition. For instance, Greco et al. (45) demonstrate that community-level traits can sometimes better explain biodiversity loss than accessibility alone. Our metric therefore identifies where hunting is likely to occur but assessing true hunting impacts will require combining this pressure layer with biodiversity data. Future efforts should aim to couple spatially explicit hunting models with ecological data to prioritize conservation actions more effectively. Furthermore, as vulnerability assessments of biodiversity expand, our maps offer a standardized and robust tool for quantifying species' exposure to HP across the tropics. This enables integration into single or multi-threat vulnerability metrics, enhancing the accuracy of biodiversity risk assessments. Similar to how Boyce et al. (46) applied climate change vulnerability metrics to marine species, our approach can support tropical terrestrial species assessments by incorporating HP as a key driver of vulnerability as an exposure layer.

Conclusions

Hunting remains one of the most understudied yet significant drivers of terrestrial biodiversity loss. Here, we address this critical knowledge gap by presenting the first global, high-resolution, and temporally explicit maps of hunting pressure across the tropics. Unlike previous species-specific or proxy-based assessments, our method uses solely ecological and socio-economic predictors to generate robust, spatially consistent predictions independent of biodiversity data, even in poorly studied regions. Our findings reveal that there are very few truly undisturbed refuges left: the “last of the wild” areas. HP is widespread, and while overall global expansion is moderate, some regions, notably Southeast Asia, West Africa, and the Atlantic Forest, have experienced sharp increases, threatening previously remote areas. By accurately identifying locations and temporal trends of hunting, our maps represent an important advance for conservation and biodiversity research. They provide the first standardized spatial layer explicitly quantifying hunting threats, enabling integration into cumulative threat maps which was previously limited by poor spatial data on overexploitation. This new resource directly supports global conservation initiatives, including extinction risk assessments, targeted interventions, and spatial prioritization aligned with the targets of the Kunming–Montreal Global Biodiversity Framework and the UN Sustainable Development Goals.

Materials and Methods

Data collection

We extended the dataset of hunting impacts on bird and mammal populations of Benítez-López et al. (2) and incorporated new sites from local hunting studies (23, 24), which were coded as 1 (hunted site) and 0 (non-hunted site). Additionally, we performed targeted searches for countries not represented in the dataset using Web of Science (detailed in *SI Appendix*), from which we extracted, when available, relevant spatial information on hunting activities, and were thus included in our dataset. Through this process, we obtained 2,463 hunted and non-hunted sites spread across the three tropical realms, Afrotropical, Indomalayan and Neotropical (*SI Appendix*, Fig. *S22*). We observed an imbalance in sites, firstly in terms of hunted (n_{Xh}=1,762) *vs.* non-hunted (n_{Xc}=701) sites, and secondly in terms of spatial distribution across biogeographical realms: 331 in the Afrotropics, 412 in the Indomalayan realm, and 1,720 in the Neotropics (see below).

We selected several socio-economic and ecological predictors known to influence hunting practices in tropical forests (3, 23, 24), including: distance to the nearest human settlement (km), distance to nearest water bodies (km), distance to protected area boundaries (km; for I-IV PAs, (47)), urban market accessibility (travel time to towns with ≥50,000 inhabitants, in minutes), availability of domestic meat as an alternative food source within 1 and 20 km^2 (kg/km^2), gross domestic product within 1 and 20 km^2 (million USD), "Human Development Index" (HDI), and human population density ($individuals/km^2$). Ecological predictors comprised forest cover (%) within 1 and 20 km^2 buffers around the site, net primary productivity (gC/m2/year), and mean slope (degrees) (see Table 1 for rationale for predictor inclusion). All predictors were masked for the pantropical forest zone, which includes areas with at least 20% forest cover (13). Except for distances to the nearest human settlement, we extracted predictor values for each study site from the raster layer at the highest available spatial resolution and by temporally matching the year of data collection reported in the study, with the year of the raster layer. The distances to the nearest settlement were extracted manually from each study using information provided by the authors (e.g., direct measure, maps) or by georeferencing hunted and non-hunted sites over satellite images. The data collected is provided with the manuscript, except for certain sites due to non-disclosure agreement for illegal hunting sites (see data availability statement).

Model building

After compiling the dataset containing site-level information, hunting status (i.e., hunted = 1; non-hunted = 0), and associated ecological and socio-economic predictors, we built supervised learning models to classify the hunting status of each site. We chose random forests for this task — a tree-based algorithm well suited for handling non-linear relationships and complex interactions among predictors, which we expected *a priori*. No spatial autocorrelation was detected in the final dataset.

To address both spatial heterogeneity and the imbalance between hunted and non-hunted sites, we implemented six different training-validation and testing strategies. Because we lacked a true out-of-sample dataset for independent validation, we used two cross-validation splitting schemes: random splitting (80% training-validation, 20% testing) and spatial blocking (block size = 5), using the *cv_spatial()* function from the blockCV R package (48). To deal with class imbalance within the training-validation datasets, we applied three approaches: SMOTE (Synthetic Minority Oversampling Technique), implemented via *smote()* in the smotefamily R package (49), class weighting to increase the importance of under-represented non-hunted sites and downsampling of the majority (hunted) class. Additionally, each model was fine-tuned using Monte Carlo cross-validation (MCCV), which is appropriate for binary classification with small sample sizes (50) (detailed in *SI Appendix*).

To further limit overfitting and increase robustness, we repeated this entire process 10 times using 10 different training-validation testing splits for each strategy. This generated ten final models per strategy. Using multiple models, rather than a single final one, allowed us to account for variability in model outcomes due to regional heterogeneity in hunting patterns, ensuring more generalizable predictions across the full tropical domain.

Model performance

We evaluated the goodness-of-fit of the fine-tuned models by comparing the observed and predicted hunting status in the testing datasets. For this, we used the *predict()* function of the randomForest R package (51) and assessed random forests performance using 5 standard metrics: Matthew correlation coefficient (MCC), F1-score, area under the Receiver Operating Curve (AUC), true positive rate (TPR) and true negative rate (TNR). These metrics were computed for each of the 10 training-validation testing splits across all six modelling strategies. We also assessed whether calibration of model predictions was necessary, following recommendations by Dormann (52) (detailed in *SI Appendix*).

Additionally, we investigated the relationships between dependent and independent predictors using two primary methods. First, we calculated the mean absolute SHAP (Shapley Additive exPlanations) values to assess the importance of each predictor. This calculation was conducted using the *sv_importance()* function from the shapviz R package (53). We examined the marginal effects of each predictor by plotting the covariate against its corresponding SHAP value for each observation from the fine-tuned models. This method allows for a clear interpretation of how each feature influences the model's predictions. Independent predictors were transformed when necessary but only for visual purposes.

Predictions

The strategy selected to predict hunting pressure (HP) across the entire pantropical forest zone at a 1 km × 1 km resolution was the one that achieved the best performance across the five goodness-of-fit metrics (see *SI Appendix*). As each modeling strategy was evaluated using multiple training-validation *vs.* testing splits, resulting in one fine-tuned random forest per split, we adopted an ensemble prediction strategy. For each grid cell, we computed the median hunting probability across all models from the best-performing approach to produce a robust, spatially explicit estimate of HP. The predictor values used for generating predictions were consistent with those previously described, except for the distance to the nearest settlement. For this predictor, we used the World Settlement Footprint dataset (54) to create distance-to-settlement layers for both 2000 and 2015, as detailed in the *SI Appendix*.

To assess temporal changes in HP, we compared model outputs between the years 2000 and 2015. This time window was chosen due to the availability of consistent and comprehensive data layers (Table 1). We quantified both the 2015 HP and the absolute difference between 2015 and 2000 values (hereafter referred to as 'change'). We identified hotspots (HP > 0.9) and refuge (HP < 0.5) of pressure and reported their extent across the tropics. We used 0.5 as the threshold to convert predicted probabilities into binary outputs, assigning 0 for values < 0.5 (no hunting) and 1 for values ≥ 0.5 (hunting), during model selection, as this was the threshold that provided the highest predictive performance across the multiple training-validation *vs.* testing splits sets.

We assessed the statistical significance of changes and realm-level differences using Student's t-tests, implemented with the *t.test()* function in R. Both one-sample and two-sample t-tests were used, applying Bonferroni corrections for multiple comparisons. Additionally, we investigated finer-scale spatial variation by aggregating values of both 2015 HP and change in HP to compute means and standard deviations at country and ecoregion levels (55).

Data availability statement

The partial dataset (excluding sites subject to non-disclosure agreements), models and scripts used in this manuscript are available at https://zenodo.org/records/15696758. Raster layers for hunting pressure and changes in hunting pressure, as well as Supplementary Tables 1, 2, and 3, are also provided in the same repository.

Acknowledgments

412 This study was supported by the EVAHUNT project (ref. CNS2023-144631) funded by the
413 MCIN/AEI/10.13039/501100011033 and the EU ("NextGenerationEU"/PRTR). IFA was supported by
414 a predoctoral research grant (PREDOC_01122) from the Junta de Andalucía.

References

1. W. J. Ripple, *et al.*, Bushmeat hunting and extinction risk to the world's mammals. *R. Soc. Open Sci.* **3**, 160498 (2016).

2. A. Benítez-López, *et al.*, The impact of hunting on tropical mammal and bird populations. *Science* **356**, 180–183 (2017).

3. J. A. Bogoni, C. A. Peres, K. M. P. M. B. Ferraz, Extent, intensity and drivers of mammal defaunation: a continental-scale analysis across the Neotropics. *Sci. Rep.* **10**, 14750 (2020).

4. C. A. Stafford, R. F. Preziosi, W. I. Sellers, A Cross-Site Analysis of Neotropical Bird Hunting Profiles. *Trop. Conserv. Sci.* **10**, 1940082917736894 (2017).

5. D. Santos-Fita, E. J. Naranjo, J. L. Rangel-Salazar, Wildlife uses and hunting patterns in rural communities of the Yucatan Peninsula, Mexico. *J. Ethnobiol. Ethnomedicine* **8**, 38 (2012).

6. B. R. Scheffers, B. F. Oliveira, I. Lamb, D. P. Edwards, Global wildlife trade across the tree of life. *Science* **366**, 71–76 (2019).

7. O. Morton, B. R. Scheffers, T. Haugaasen, D. P. Edwards, Impacts of wildlife trade on terrestrial biodiversity. *Nat. Ecol. Evol.* **5**, 540–548 (2021).

8. D. W. S. Challender, *et al.*, Identifying species likely threatened by international trade on the IUCN Red List can inform CITES trade measures. *Nat. Ecol. Evol.* **7**, 1211–1220 (2023).

9. R. A. Senior, B. F. Oliveira, J. Dale, B. R. Scheffers, Wildlife trade targets colorful birds and threatens the aesthetic value of nature. *Curr. Biol.* **32**, 4299-4305.e4 (2022).

10. L. J. Hughes, O. Morton, B. R. Scheffers, D. P. Edwards, The ecological drivers and consequences of wildlife trade. *Biol. Rev.* **98**, 775–791 (2023).

11. L. J. Hughes, *et al.*, Global hotspots of traded phylogenetic and functional diversity. *Nature* **620**, 351–357 (2023).

12. R. J. Almeida, A. N. Mazza, J. L. Lockwood, Does fortune follow function? Exploring how consumer preferences drive the functional trait composition of the global songbird trade. *People Nat.* **6**, 1366–1377 (2024).

13. P. Potapov, *et al.*, The last frontiers of wilderness: Tracking loss of intact forest landscapes from 2000 to 2013. *Sci. Adv.* **3**, e1600821 (2017).

14. O. Venter, *et al.*, Sixteen years of change in the global terrestrial human footprint and implications for biodiversity conservation. *Nat. Commun.* **7**, 12558 (2016).

15. Y. Malhi, T. A. Gardner, G. R. Goldsmith, M. R. Silman, P. Zelazowski, Tropical Forests in the Anthropocene. *Annu. Rev. Environ. Resour.* **39**, 125–159 (2014).

16. O. Venter, *et al.*, Global terrestrial Human Footprint maps for 1993 and 2009. *Sci. Data* **3**, 160067 (2016).

17. H. S. Grantham, *et al.*, Anthropogenic modification of forests means only 40% of remaining forests have high ecosystem integrity. *Nat. Commun.* **11**, 5978 (2020).

18. L. N. Joppa, *et al.*, Filling in biodiversity threat gaps. *Science* **352**, 416–418 (2016).

19. K. H. Redford, The Empty Forest: Many large animals are already ecologically extinct in vast areas of neotropical forest where the vegetation still appears intact. *BioScience* **42**, 412–422 (1992).

20. D. S. Wilkie, E. L. Bennett, C. A. Peres, A. A. Cunningham, The empty forest revisited. *Ann. N. Y. Acad. Sci.* **1223**, 120–128 (2011).

21. R. Dirzo, *et al.*, Defaunation in the Anthropocene. *Science* **345**, 401–406 (2014).

22. S. Ziegler, *et al.*, Mapping Bushmeat Hunting Pressure in Central Africa. *Biotropica* **48**, 405–412 (2016).

23. A. Benítez-López, L. Santini, A. M. Schipper, M. Busana, M. A. J. Huijbregts, Intact but empty forests? Patterns of hunting-induced mammal defaunation in the tropics. *PLOS Biol.* **17**, e3000247 (2019).

24. I. Ferreiro-Arias, *et al.*, Drivers and spatial patterns of avian defaunation in tropical forests. *Divers. Distrib.* **31**, e13855 (2025).

25. M. B. J. Harfoot, *et al.*, Using the IUCN Red List to map threats to terrestrial vertebrates at global scale. *Nat. Ecol. Evol.* **5**, 1510–1519 (2021).

26. J. Riggio, *et al.*, Global human influence maps reveal clear opportunities in conserving Earth's remaining intact terrestrial ecosystems. *Glob. Change Biol.* **26**, 4344–4356 (2020).

27. M. Pacifici, A. Cristiano, G. Mancini, D. Nania, M. Davoli, Global hotspots of bushmeat hunting risk for mammals. [Preprint] (2025). Available at: https://www.researchsquare.com/article/rs-6278255/v1 [Accessed 20 June 2025].

28. A. Hughes, M. C. Orr, R. D. Palacio, Y. Xuan, H. Qiao, A dire need for better standards of data quality, transparency, and reproducibility in IUCN RedList assessments. (2024).

29. A. Hughes, M. Orr, R. Palacio, Y. Xuan, H. Qiao, Citation needed: Biased and missing data weaken the IUCN Red List of species. [Preprint] (2025). Available at: https://www.authorea.com/users/836019/articles/1260455-citation-needed-biased-and-missing-data-weaken-the-iucn-red-list-of-species?commit=32085b54cf8741bc3ba6792baad289b61482b53a [Accessed 10 June 2025].

30. D. J. Ingram, *et al.*, Regional patterns of wild animal hunting in African tropical forests. *Nat. Sustain.* **8**, 202–214 (2025).

31. J. Ma, J. Li, W. Wu, J. Liu, Global forest fragmentation change from 2000 to 2020. *Nat. Commun.* **14**, 3752 (2023).

32. V. R. V. Nguimdo, *et al.*, Long-Term Monitoring of Hunting Signs Reveals Complex Spatiotemporal Patterns of Hunting Activities in an Unprotected African Rainforest. *Divers. Distrib.* **31**, e13951 (2025).

33. A. Semper-Pascual, *et al.*, Occurrence dynamics of mammals in protected tropical forests respond to human presence and activities. *Nat. Ecol. Evol.* **7**, 1092–1103 (2023).

34. I. M. Redmond, Recipes for Survival: Controlling the Bushmeat Trade. Ape Alliance report funded by WSPA. *Ape Alliance Rep.* (2006).

35. D. Liang, X. Giam, S. Hu, L. Ma, D. S. Wilcove, Assessing the illegal hunting of native wildlife in China. *Nature* **623**, 100–105 (2023).

36. O. Wedage, *et al.*, Specialized rainforest hunting by Homo sapiens ~45,000 years ago. *Nat. Commun.* **10**, 739 (2019).

37. J. F. Brodie, *et al.*, Landscape-scale benefits of protected areas for tropical biodiversity. *Nature* **620**, 807–812 (2023).

38. C. A. Peres, Synergistic Effects of Subsistence Hunting and Habitat Fragmentation on Amazonian Forest Vertebrates. *Conserv. Biol.* **15**, 1490–1505 (2001).

39. R. Sreekar, *et al.*, The use of species–area relationships to partition the effects of hunting and deforestation on bird extirpations in a fragmented landscape. *Divers. Distrib.* **21**, 441–450 (2015).

40. G. Mancini, *et al.*, Synergistic effects of habitat fragmentation and hunting on the extinction risk of neotropical primates. *Biodivers. Conserv.* **32**, 2655–2669 (2023).

41. J. S. Sze, D. Z. Childs, L. R. Carrasco, D. P. Edwards, Indigenous lands in protected areas have high forest integrity across the tropics. *Curr. Biol.* **32**, 4949-4956.e3 (2022).

42. A. J. Plumptre, *et al.*, Where Might We Find Ecologically Intact Communities? *Front. For. Glob. Change* **4** (2021).

43. L. Mair, *et al.*, A metric for spatially explicit contributions to science-based species targets. *Nat. Ecol. Evol.* **5**, 836–844 (2021).

44. C. A. Emogor, *et al.*, Pangolin hunting in southeast Nigeria is motivated more by local meat consumption than international demand for scales. *Nat. Ecol. Evol.* 1–10 (2025). https://doi.org/10.1038/s41559-025-02734-3.

45. I. Greco, *et al.*, Landscape-level human disturbance results in loss and contraction of mammalian populations in tropical forests. *PLOS Biol.* **23**, e3002976 (2025).

46. D. G. Boyce, *et al.*, A climate risk index for marine life. *Nat. Clim. Change* **12**, 854–862 (2022).

47. S. L. Maxwell, *et al.*, Area-based conservation in the twenty-first century. *Nature* **586**, 217–227 (2020).

48. R. Valavi, J. Elith, J. J. Lahoz-Monfort, G. Guillera-Arroita, blockCV: An r package for generating spatially or environmentally separated folds for k-fold cross-validation of species distribution models. *Methods Ecol. Evol.* **10**, 225–232 (2019).

49. W. Siriseriwan, smotefamily: A Collection of Oversampling Techniques for Class Imbalance Problem Based on SMOTE. https://doi.org/10.32614/CRAN.package.smotefamily. Deposited 8 September 2016.

50. G. Shan, Monte Carlo cross-validation for a study with binary outcome and limited sample size. *BMC Med. Inform. Decis. Mak.* **22**, 270 (2022).

51. A. Liaw, M. Wiener, Classification and Regression by randomForest.

52. C. F. Dormann, Calibration of probability predictions from machine-learning and statistical models. *Glob. Ecol. Biogeogr.* **29**, 760–765 (2020).

53. M. Mayer, shapviz: SHAP Visualizations. https://doi.org/10.32614/CRAN.package.shapviz. Deposited 10 June 2022.

54. M. Marconcini, A. Metz- Marconcini, T. Esch, N. Gorelick, Understanding Current Trends in Global Urbanisation - The World Settlement Footprint Suite. *GI_Forum* **1**, 33–38 (2021).

55. D. M. Olson, *et al.*, Terrestrial Ecoregions of the World: A New Map of Life on Earth: A new global map of terrestrial ecoregions provides an innovative tool for conserving biodiversity. *BioScience* **51**, 933–938 (2001).

56. J.-F. Pekel, A. Cottam, N. Gorelick, A. S. Belward, High-resolution mapping of global surface water and its long-term changes. *Nature* **540**, 418–422 (2016).

57. H. C. Bingham, *et al.*, User Manual for the World Database on Protected Areas and world database on other effective area- based conservation measures: 1.6.

58. A. Nelson, Estimated travel time to the nearest city of 50,000 or more people in year 2000. Global Environment Monitoring Unit - Joint Research Centre of the European Commission, Ispra Italy (2008).

59. D. J. Weiss, *et al.*, A global map of travel time to cities to assess inequalities in accessibility in 2015. *Nature* **553**, 333–336 (2018).

60. M. Gilbert, *et al.*, Global distribution data for cattle, buffaloes, horses, sheep, goats, pigs, chickens and ducks in 2010. *Sci. Data* **5**, 180227 (2018).

61. J. S. Brashares, C. D. Golden, K. Z. Weinbaum, C. B. Barrett, G. V. Okello, Economic and geographic drivers of wildlife consumption in rural Africa. *Proc. Natl. Acad. Sci.* **108**, 13931–13936 (2011).

62. J. Chen, *et al.*, Global 1 km × 1 km gridded revised real gross domestic product and electricity consumption during 1992–2019 based on calibrated nighttime light data. *Sci. Data* **9**, 202 (2022).

63. M. Kummu, M. Taka, J. H. A. Guillaume, Gridded global datasets for Gross Domestic Product and Human Development Index over 1990–2015. *Sci. Data* **5**, 180004 (2018).

64. Center For International Earth Science Information Network-CIESIN-Columbia University, Gridded Population of the World, Version 4 (GPWv4): Population Density, Revision 11. Palisades, NY: Socioeconomic Data and Applications Center (SEDAC). https://doi.org/10.7927/H49C6VHW. Deposited 2017.

65. P. Potapov, *et al.*, The Global 2000-2020 Land Cover and Land Use Change Dataset Derived From the Landsat Archive: First Results. *Front. Remote Sens.* **3** (2022).

66. S. W. Running, M. Zhao, Daily GPP and Annual NPP (MOD17A2H/A3H) and Year-end Gap- Filled (MOD17A2HGF/A3HGF) Products NASA Earth Observing System MODIS Land Algorithm (For Collection 6.1).

67. G. Amatulli, *et al.*, A suite of global, cross-scale topographic predictors for environmental and biodiversity modeling. *Sci. Data* **5**, 180040 (2018).

Figures and Tables

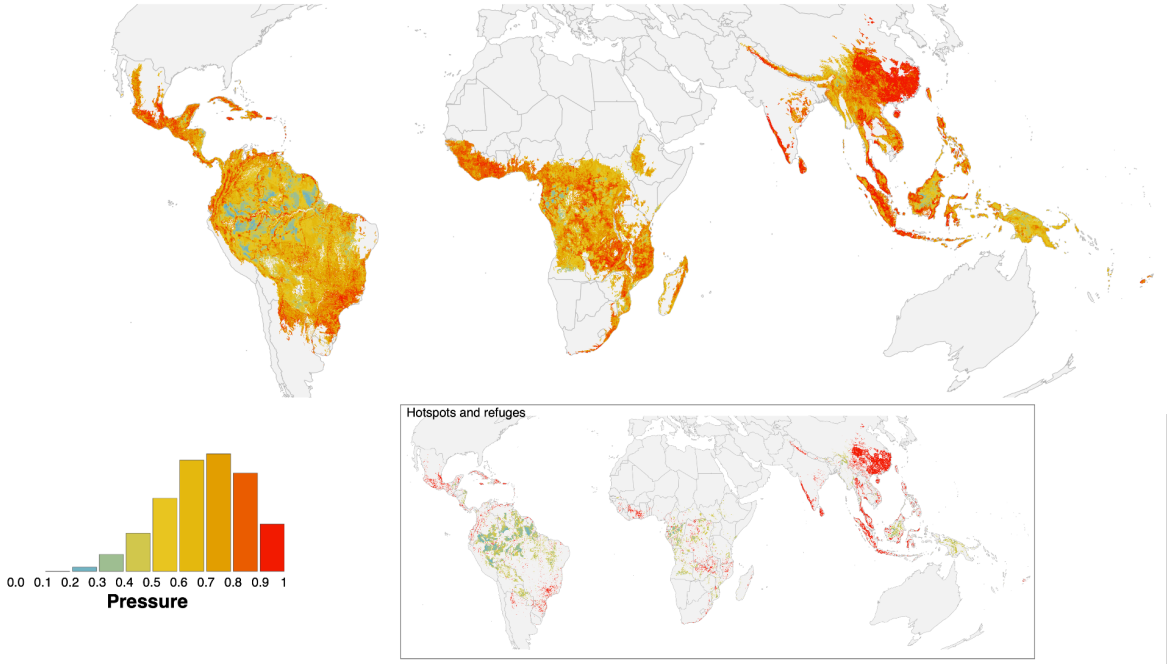

Figure 1. Spatial variation in predicted hunting pressure across tropical forests in 2015. Hunting pressure corresponds to probability of a site of being hunted and was predicted for each 1 km × 1 km grid cell using spatially explicit environmental and socio-economic predictors from ca. 2015. Predictions represent the median values from 10 independently trained and fine-tuned random forest models, each calibrated using random cross-validation and downsampling to address class imbalance (hunted vs. non-hunted sites). Hunting pressure is displayed on a continuous scale from 0 to 1, with color breaks at 0.1 intervals. The inset highlights the same map but displays only grid cells with pressure above 0.9 (in red), representing hotspots, and those below 0.5 (in green), representing potential refuges.

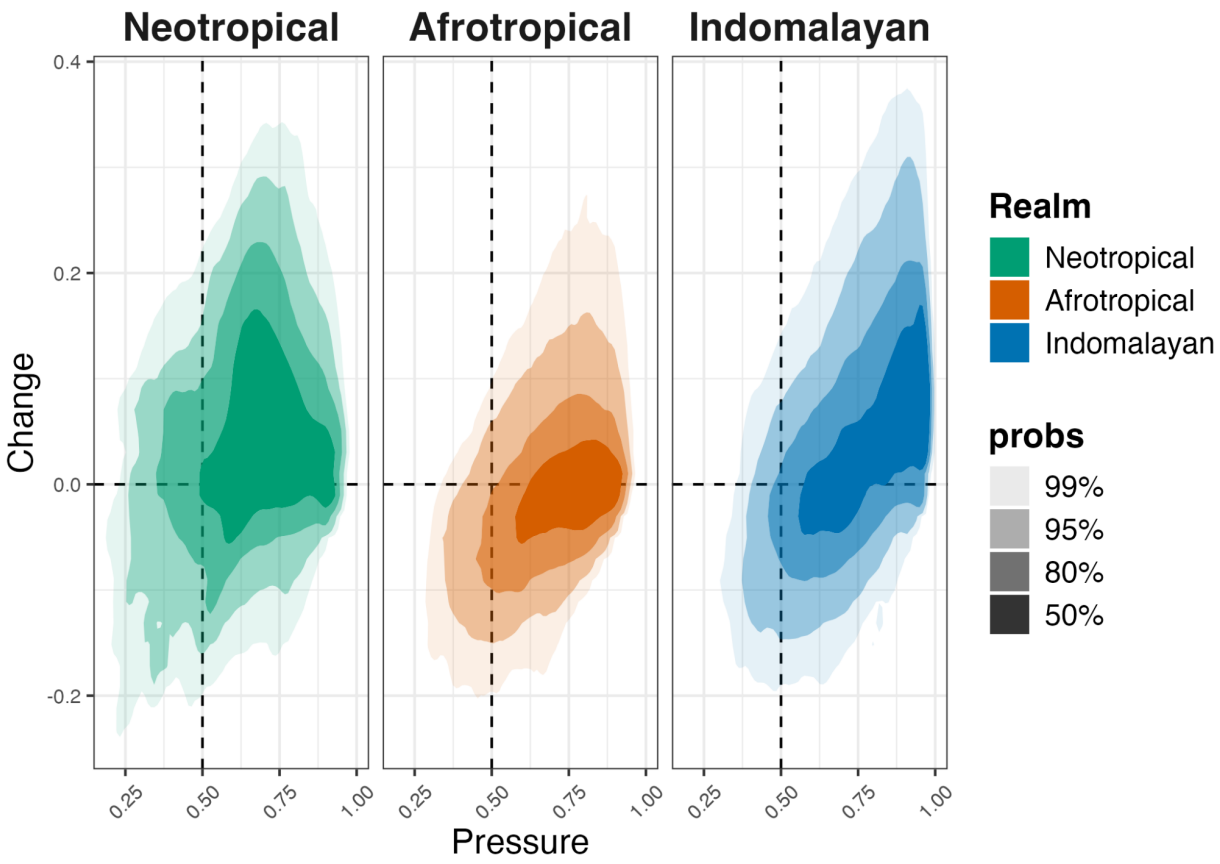

Figure 2. Spatio-temporal variation in predicted hunting pressure across tropical forests between 2000 and 2015, by biogeographic realm. Each box shows the density distribution of predicted hunting pressure in 2015 (pressure) and the change in pressure between 2000 and 2015 (change) across 1 km × 1 km grid cells within each biogeographic realm. Change is calculated as the difference between predicted pressure in 2015 and 2000, where negative values indicate a decrease and positive values an increase in pressure. Color intensity represents the relative probability density, ranging from darker shades (values around the median, with ~50% of cells) to lighter shades (covering up to 99% of the observed values).

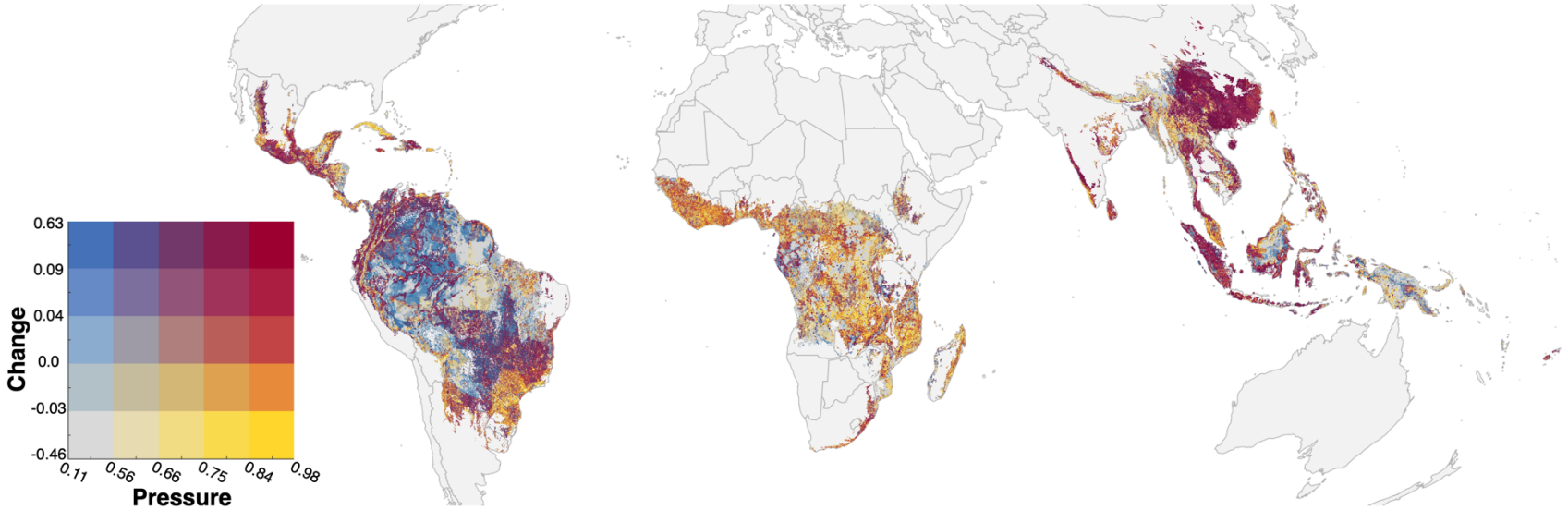

Figure 3. Spatio-temporal variation in predicted hunting pressure across tropical forests between 2000 and 2015. Hunting pressure corresponds to probability of a site of being hunted and was predicted at a 1 km × 1 km resolution using spatially explicit environmental and socio-economic predictors from 2000 and 2015 (or the closest available years). Predictions correspond to the median values from 10 independently trained and fine-tuned random forest models, calibrated using random cross-validation and downsampling to correct for class imbalance (hunted vs. non-hunted sites). The pressure values represent predicted hunting pressure in 2015, while change values indicate the difference between 2015 and 2000 predictions, where negative values reflect a decrease and positive values an increase in pressure over time. Both metrics are categorized by percentiles (0–20%, 20–40%, 40–60%, 60–80%, 80–100%). Combinations of pressure and change quantiles are color-coded as grey: low pressure and decreasing pressure, yellow: high pressure and decreasing pressure, blue: low pressure and increasing pressure or purple: high pressure and increasing pressure.

598 **Table 1. Predictors used in the models, with data sources, temporal and spatial resolution, and its expected relationship with hunting**
599 **pressure**

Predictor	Expected relationships	Reference	Approximate spatial resolution	Collecting years
Distance to the nearest human settlement	According to the central place foraging hypothesis, decaying hunting pressure is usually related to the distance to small towns and villages. Hence, we expect that hunting pressure would decrease with distance to human settlements.	(54)	30 m x 30 m 10 m x 10 m	2000, 2015
Distance to the nearest water body		(56)	distance	2024
Minimum distance to protected area (PA) boundaries	PAs may attract hunters due to higher wildlife abundance but also benefit from enforcement. We therefore expected hunting pressure to peak at PA edges and decline beyond.	(57)	distance	2000 - 2024
Accessibility to urban markets	Travel time to major towns is commonly used as a proxy for accessibility to urban markets, where wildlife products such as bushmeat, animal parts, or live animals can be sold. Shorter travel times reduce the costs and effort required to transport hunted goods, thereby increasing the incentive for hunters to operate in those areas. As a result, areas closer to major towns are generally associated with higher hunting pressure driven by commercial trade.	(58, 59)	1 km x 1 km	2000, 2015
Availability to domestic meat	Greater availability of domestic meat is expected to reduce reliance on wild meat for subsistence, as it provides an accessible and reliable alternative protein source. This shift in dietary dependence may lead communities to hunt less, particularly in areas where hunting is primarily driven by the need for food rather than commercial trade, thereby reducing overall hunting pressure.	(60)	1 km x 1 km 20 km x 20 km	2010
Gross domestic product	The relationship between hunting and wealth is complex and context-dependent, often varying between rural and urban settings (61). In rural areas, wildlife meat consumption tends to decline with increasing wealth, while in urban areas, it may increase due to demand for exotic or luxury products. Additionally, wildlife trade can serve as a significant income source for rural communities, especially in	(62)	1 km x 1 km 20 km x 20 km	2000 - 2020

Human development index	remote areas where rare species can fetch high market prices. Considering these factors, we expected higher hunting pressure in poorer regions due to subsistence needs, but also some positive association with wealthier areas where wildlife products are valued as luxury commodities.	(63)	regional scale	1990 - 2015
Human population density	Hunting pressure is typically higher in healthier, less-degraded forests, where wildlife is more abundant and easier to encounter. These areas also tend to support rarer, specialist species that can be specifically targeted due to their high market value, further increasing hunting activity.	(64)	1kmx1km	2000, 2005, 2010, 2015, 2020
Forest cover		(65)	30 m x 30 m	2000, 2005, 2010, 2015, 2020
Net primary productivity		(66)	1 km x 1 km	2001 - 2021
Elevation and ground slope	Hunting pressure is generally lower in steep, less accessible areas due to the physical difficulty of reaching these sites and the typically lower abundance of wildlife, making hunting less efficient and less rewarding.	(67)	1 km x 1 km	2024

600

Supplementary Information

Supplementary Methods

Data collection

To improve data coverage and reduce spatial biases, we conducted additional data mining focused on these regions. For this, we used the following search string in Web of Science: "(road* OR settlement* OR village OR access* OR distance OR proximity OR impact OR effect) AND (hunt OR bushmeat OR wild meat OR poach* OR trade OR snare*) AND (wildlife OR vertebr* OR mammal* OR bird* OR avian) AND (tropic* forest OR ecosystem*) AND (Vietnam OR China OR Laos OR Taiwan OR Philippines OR Cambodia OR India OR Papua New Guinea OR Borneo OR Java OR Sri Lanka OR Myanmar OR Mozambique OR Madagascar OR Nigeria OR Cuba OR Puerto Rico OR Dominican Republic OR Trinidad and Tobago OR Sao Tome OR Mauritius)". This search returned 1,509 hits, from which we extracted relevant spatial information on hunting activities and were thus included in our dataset. Additionally, sites with missing values for some predictors (detailed in the main manuscript) were removed and the remaining sites were manually checked to ensure that forest cover was reliable for the site.

Model building

Monte Carlo Cross-Validation (MCCV) involved 100 iterations of randomly splitting the training-validation data into 70% training and 30% validation. For each iteration, we assessed model performance using the mean log loss between observed and predicted hunting status. The best model was then trained on the full training-validation dataset using the hyperparameters that minimized the average log loss across all 100 splits using the *randomForest()* function of the randomForest R package (Liaw & Wiener, 2002). Model training and prediction for the MCCV were performed using the *ranger()* and *predict()* functions from the ranger R package (Wright et al., 2015). We chose *randomForest()* to train the fine-tuned model because the *predict()* function of the randomForest R package outperformed the one of the ranger R package in terms of computation times.

Model performance

Prior to predicting hunting pressure across the pantropical forest zone, we checked if calibration was needed for each model's predictions, i.e., prediction obtained from the fine-tuned models for the test dataset, to facilitate probabilistic interpretation and mitigate overfitting — a crucial step to prevent a complete dichotomy between hunted and non-hunted sites. We used generalized linear models with a binomial distribution, fitting them to the observed site type (hunted or non-hunted) using the *glm()* function. Once the models were appropriately fitted, we used them to re-predict hunting pressure, using the same predictive values. These recalibrated predictions were then compared against observed hunting status to check calibration.

Predictions

To compute the raster layer measuring the distance to the nearest protected area at a 1 km × 1 km resolution, we calculated distances based on the centroid of each grid cell. Specifically, for every 1 km × 1 km grid cell across the tropics, we determined the absolute distance from its centroid to the nearest boundary of a protected area. This calculation was performed sequentially using the *sf_join()* function (with the parameter "join = st_nearest_feature") and the *st_distance()* function from the sf R package (Pebesma, 2018).

Distances to human settlements were calculated for each 1 km × 1 km grid cell using the World Settlement Footprint (WSF®) dataset (Marconcini et al., 2021), which provides high-resolution (30 m × 30 m) annual settlement data from 1985 to 2015. We aggregated these settlement pixels to the 1 km grid scale by classifying grid cells as '1' if they contained any settlement pixel, or '0' otherwise. Grid cells containing at least one settlement pixel, classified as '1', were assigned zero. For grid cells classified as '0' (no settlements), we computed the distance to the nearest settlement cell. Before distance calculations, urban settlements and settlements located close to cities (travel time < 5 min to major towns, following Weiss et al., 2015) or on artificial land-use types (Copernicus Land Cover maps) were excluded. Distance computations were performed using an equal-area Mollweide projection.

Other data layers were directly utilized without modification, except for certain regional predictors that required aggregation. Specifically, gross domestic product (GDP), population density, and livestock biomass were aggregated accordingly, as was the forest cover percentage, which were aggregated over areas equivalent to buffer zones of 1 km and 20 km radius, respectively.

Realm-specific models

In addition to the global models, we also fine-tuned and trained separate random forest models for each tropical realm by filtering the dataset accordingly. These realm-specific models followed the same framework and procedures as the global model. In this *SI Appendix*, we provide the corresponding results for model performance (goodness-of-fit metrics) and the relationships between predictors and the probability of hunting (Fig. S15-S21)

Supplementary Results

Model performance

The model presented in the main article was selected based on superior performance across several goodness-of-fit metrics: Matthew correlation coefficient (MCC), F1-score, accuracy, area under the receiving operating curve (AUC), true positive rate (TPR), and true negative rate (TNR); and its capacity to effectively represent spatial variations in hunting pressure. Among the various tested strategies, random splitting combined with

either downsampling or class weighting methods to address class imbalance yielded the best predictive performance, demonstrating consistently high and stable results across the 10 random forests (Fig. S1).

However, the distribution of predicted values before and after calibration differed notably between downsampling and class-weighting. Downsampling exhibited greater variance and less skewed predictions compared to class weighting (Fig. S2 and S3). Calibration did not negatively affect goodness-of-fit metrics and improved the correlation between observed and predicted hunting pressure values (Fig. S4 and S5). Based on these findings, we presented, in the result section, the results obtained with calibrated random forests trained with random splitting and combined with downsampling. For transparency, additional maps from uncalibrated models are also provided.

Supplementary Figures

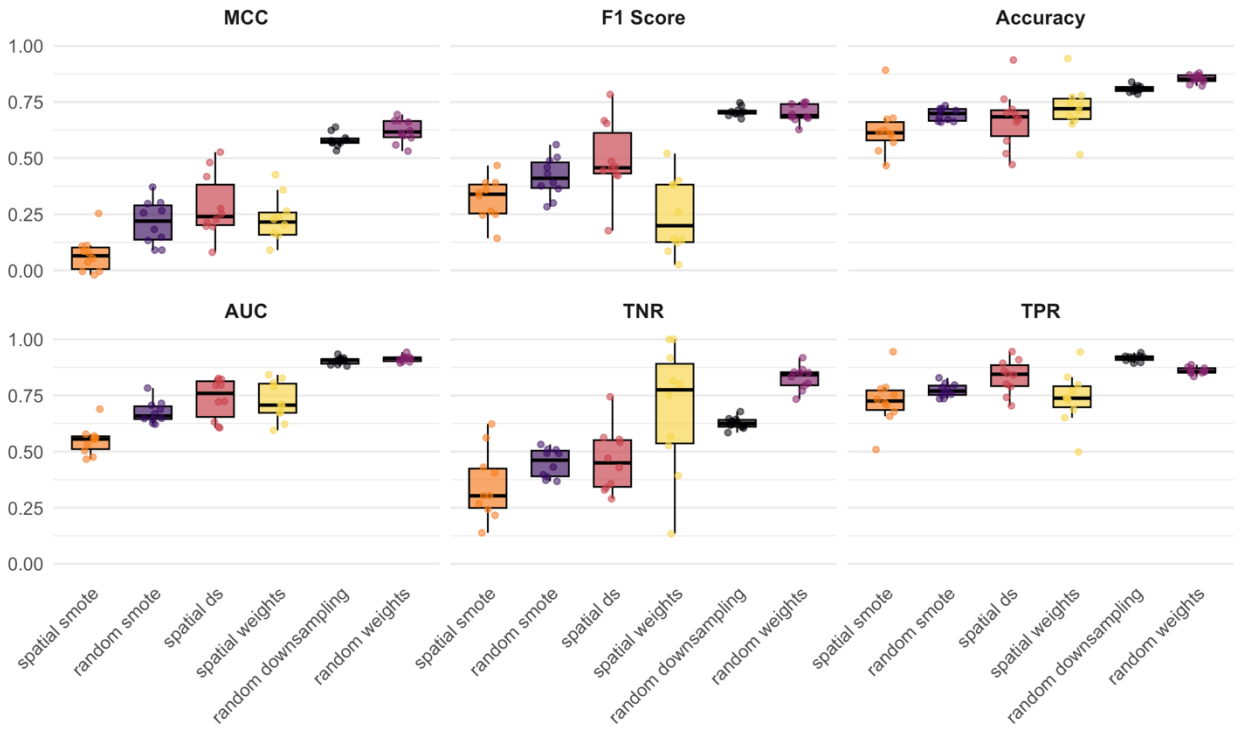

Figure S1. Goodness-of-fit metrics for six supervised learning approaches during the testing phase. We evaluated the performance of six modeling strategies, combining two data-splitting methods, random k-fold cross-validation and spatial blocking, with three approaches for handling class imbalance: class weighting, downsampling, and SMOTE. For each strategy, 10 random forest models were trained, with training-validation and testing datasets generated either randomly or using spatial blocking. Model performance was assessed using six key metrics: Matthew correlation coefficient (MCC), F1-score, accuracy, area under the receiving operating curve (AUC), true positive rate (TPR), and true negative rate (TNR). These metrics were calculated

by comparing observed and predicted site classifications (hunted vs non-hunted) in the testing datasets, following model fine-tuning on the training-validation sets using Monte Carlo cross-validation to optimize hyperparameters.

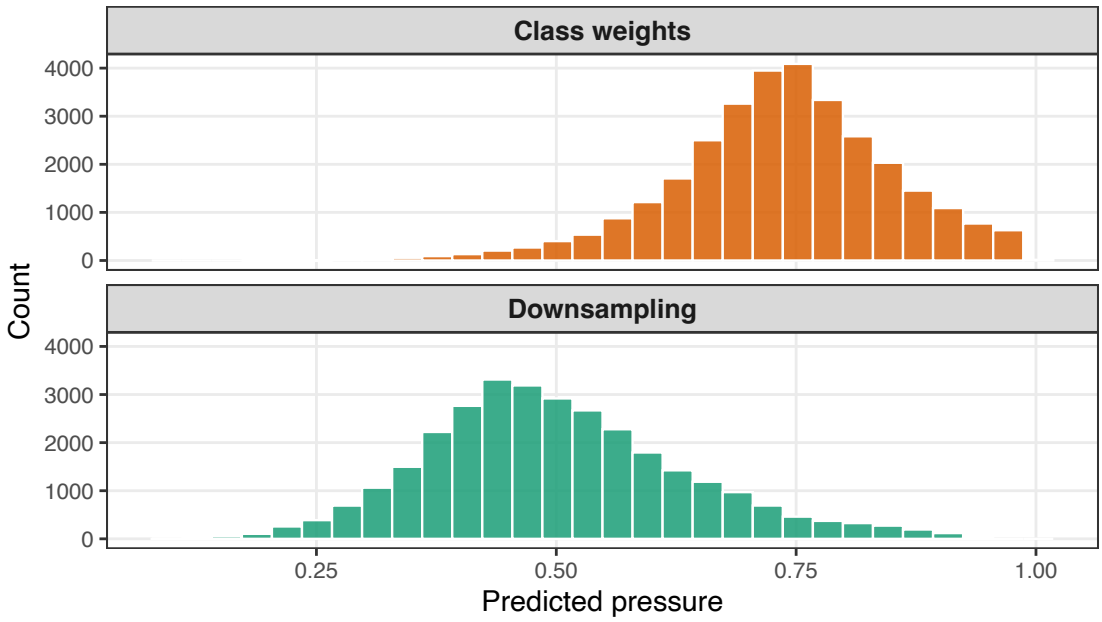

Figure S2. Distribution of predicted hunting pressure values (without calibration) under two approaches for handling class imbalance: downsampling and class weighting. Both models were trained using random k-fold cross-validation.

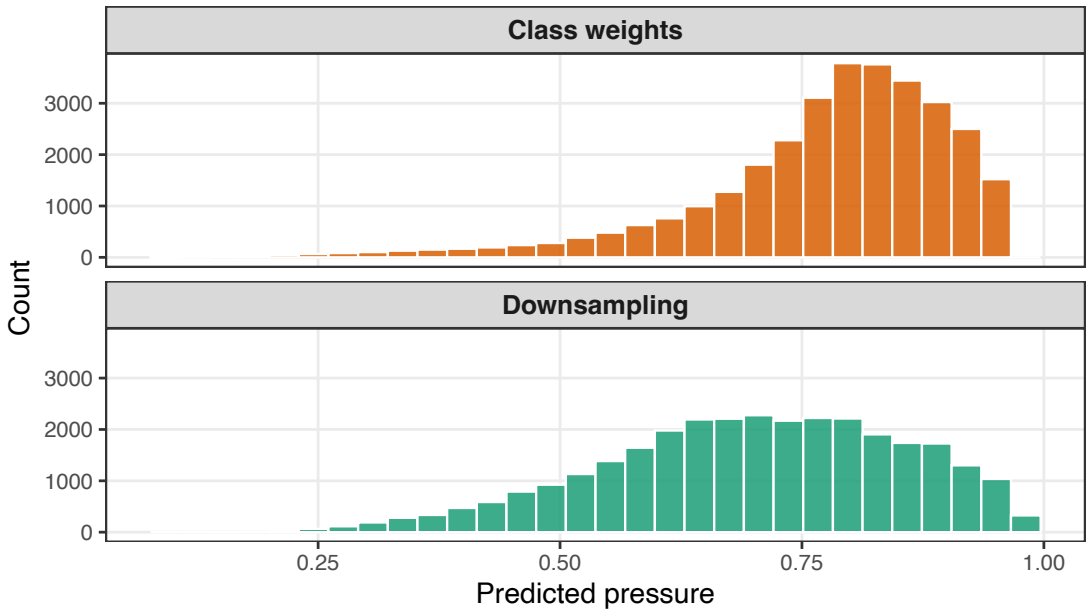

Figure S3. Distribution of predicted hunting pressure values (with calibration) under two approaches for handling class imbalance: downsampling and class weighting. Both models were trained using random k-fold cross-validation.

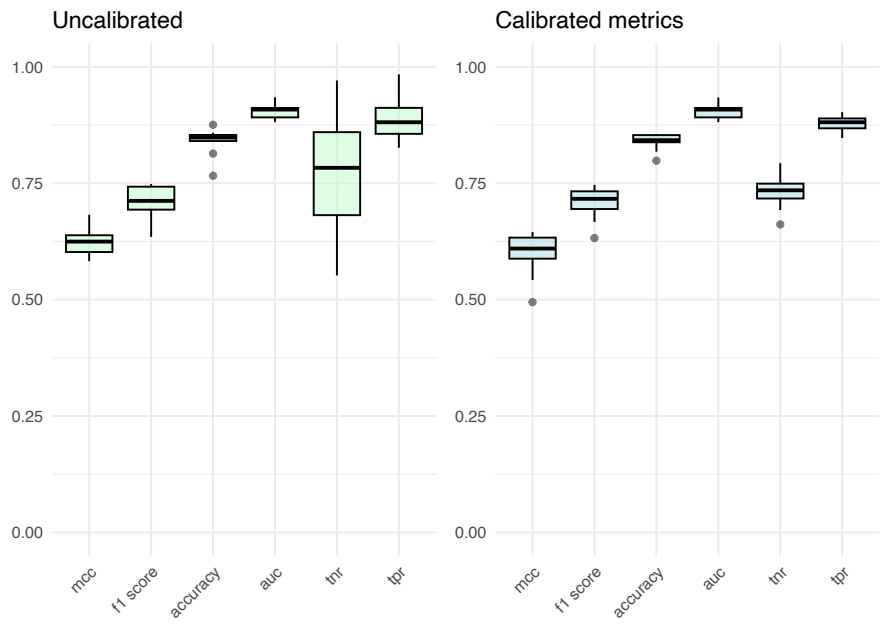

Figure S4. Comparison of goodness-of-fit metrics between uncalibrated and calibrated supervised learning models. Both approaches use random k-fold cross-validation and downsampling to address class imbalance.

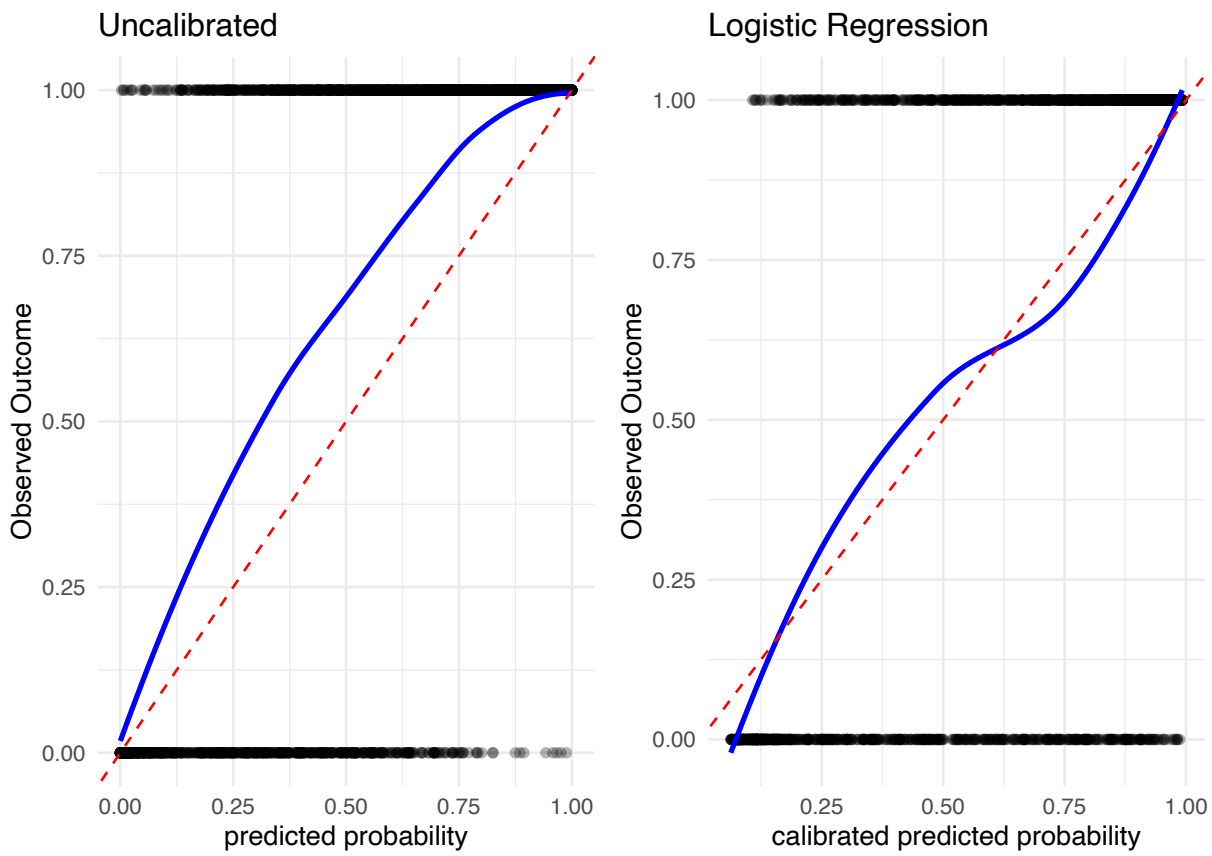

Figure S5. Comparison between observed and predicted values for uncalibrated and calibrated supervised learning models. Both approaches use random k-fold cross-validation and downsampling to address class imbalance.

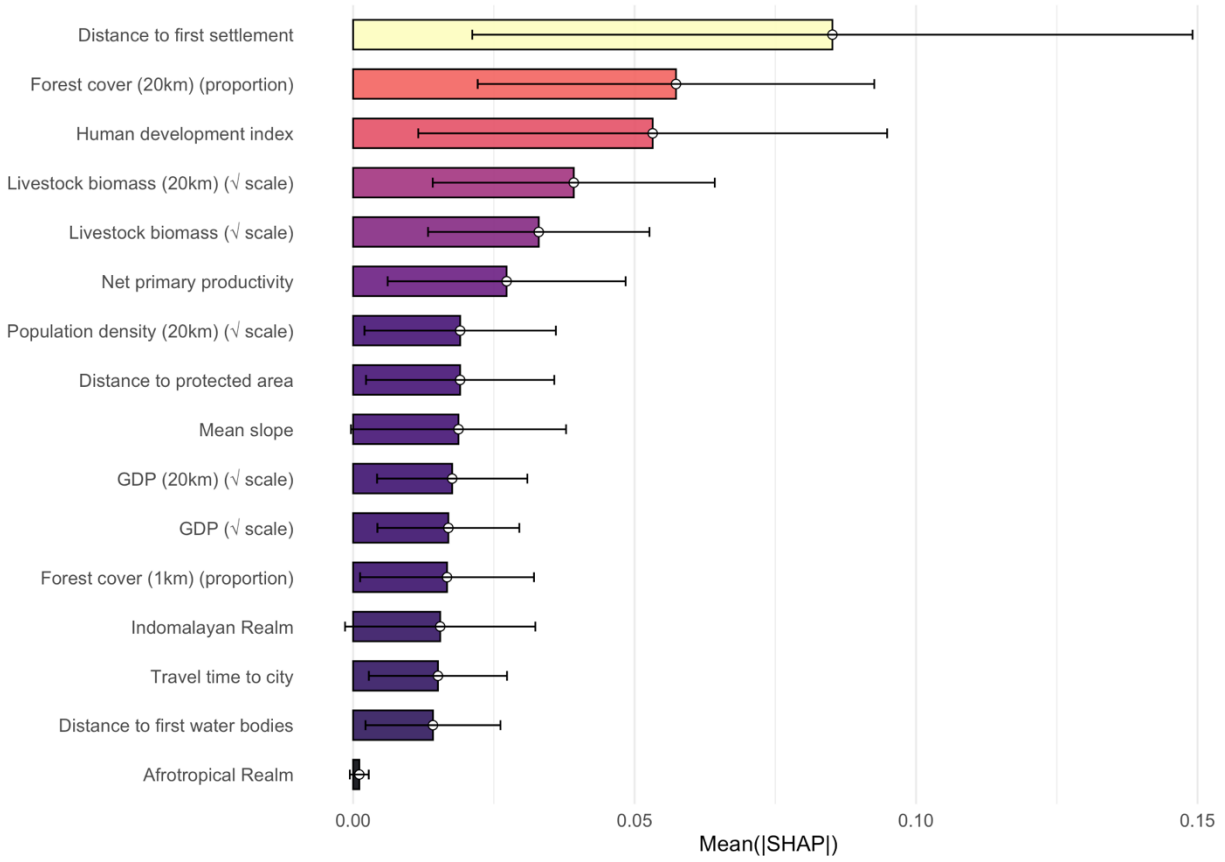

Figure S6. Global importance of ecological and socio-economic predictors in 10 random forest models. Mean absolute SHAP (SHapley Additive exPlanations) values are displayed to summarize the overall importance of each predictor across models. The brackets represent the standard deviation and the white dot the mean.

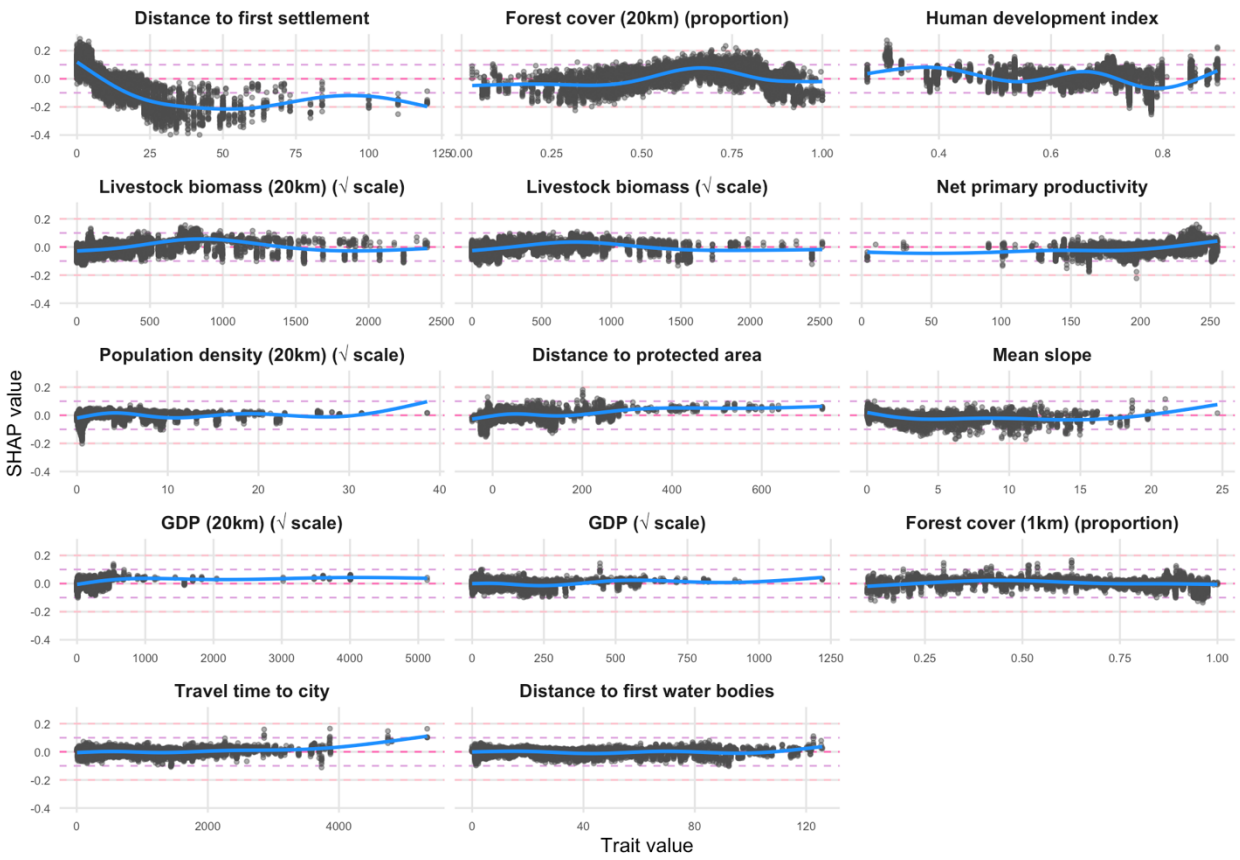

Figure S7. Marginal effects of ecological and socio-economic predictors in 10 random forest models using downsampling. SHAP values were used to assess the importance of each predictor on the predicted probability of a site being classified as hunted (i.e., hunting pressure). Each point represents a prediction for an individual site, based on ecological and socio-economic predictors, using the previously trained random forest classifiers. Positive SHAP values indicate that a given predictor increases the likelihood of a site being classified as hunted, while negative SHAP values suggest an association with non-hunted status. A non-linear regression line is included to visualize the shape of each predictor's importance. Additionally, mean absolute SHAP values are displayed to summarize the overall importance of each predictor across models.

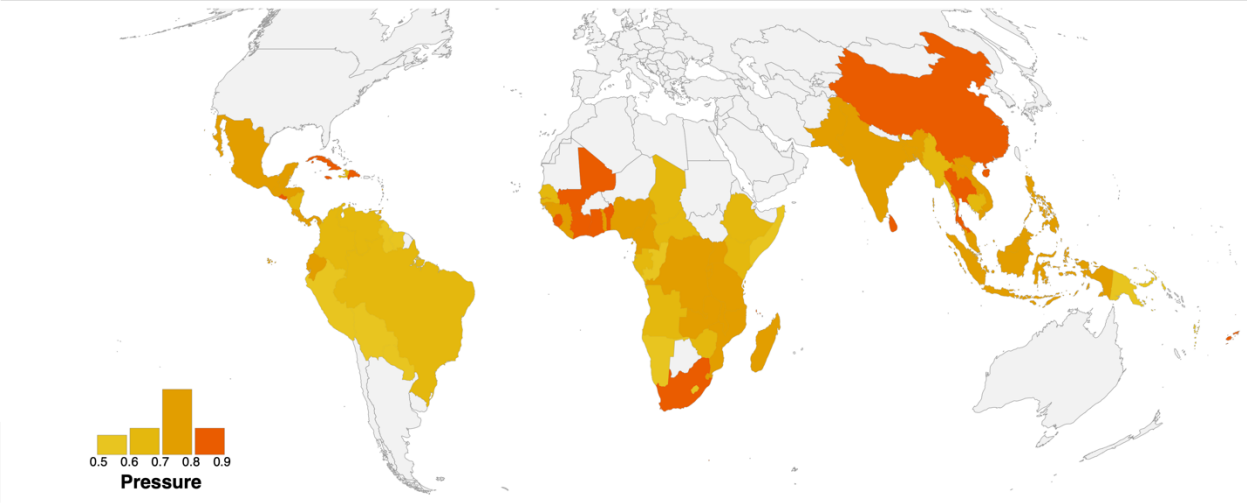

Figure S8. Spatial variation in predicted hunting pressure in tropical forests across countries in 2015. Hunting pressure was predicted for each 1 km × 1 km grid cell using spatially explicit environmental and socio-economic predictors from 2015 (or the closest available year) and aggregated by country to provide a mean value of pressure per country. Predictions represent the median values from 10 independently trained and fine-tuned random forest models, each calibrated using random k-fold cross-validation and downsampling to address class imbalance (hunted vs. non-hunted sites). Hunting pressure is displayed on a continuous scale from 0 to 1, with color breaks at 0.1 intervals.

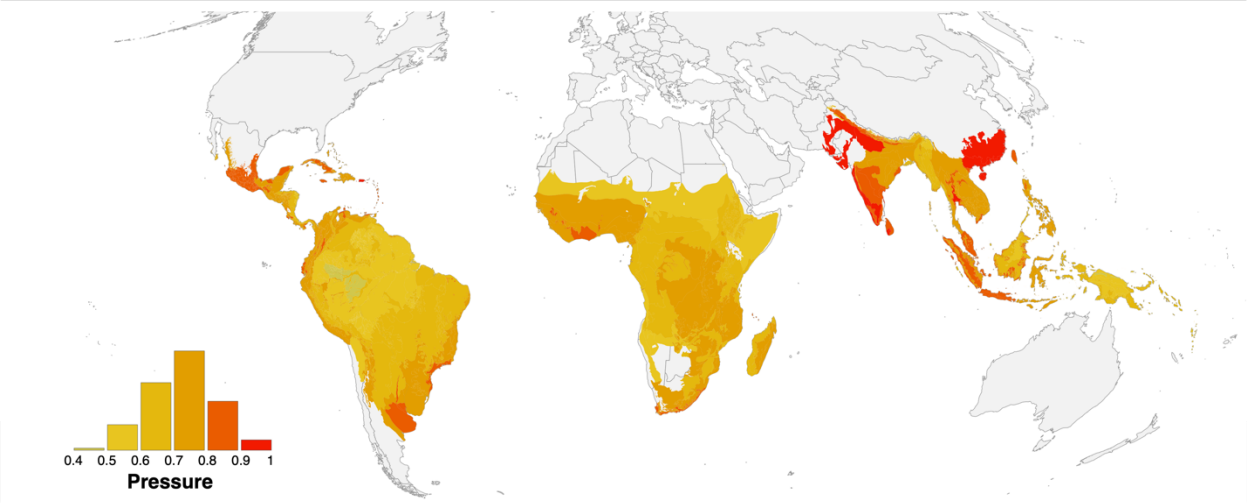

Figure S9. Spatial variation in predicted hunting pressure in tropical forests across ecoregion in 2015. Hunting pressure was predicted for each 1 km × 1 km grid cell using spatially explicit environmental and socio-economic predictors from 2015 (or the closest available year) and aggregated by ecoregion to provide a mean value of pressure per ecoregion. Predictions represent the median values from 10 independently trained and fine-tuned random forest models, each calibrated using random k-fold cross-validation and downsampling to address class imbalance (hunted vs. non-hunted sites). Hunting pressure is displayed on a continuous scale from 0 to 1, with color breaks at 0.1 intervals.

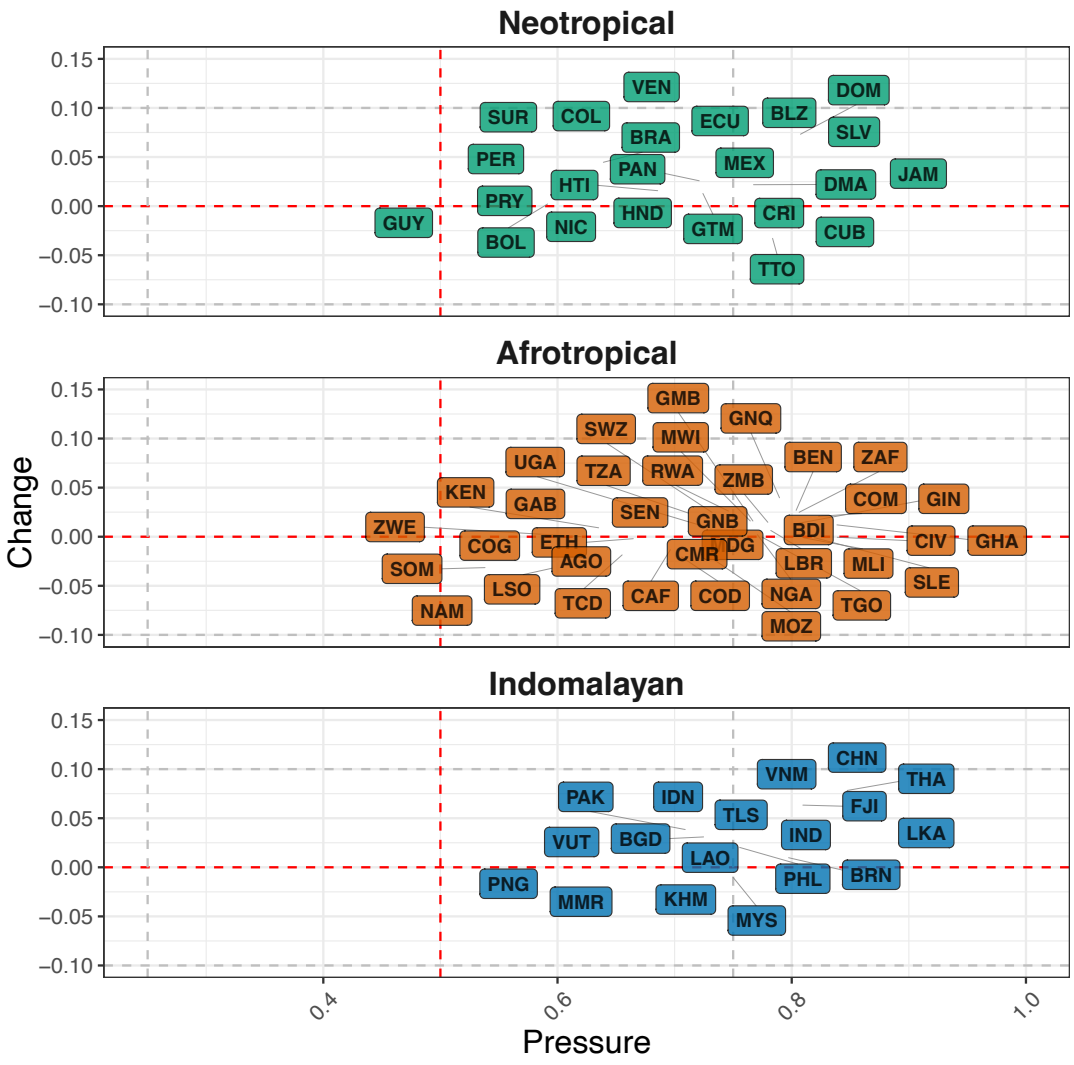

Figure S10. Spatio-temporal variation in predicted hunting pressure in tropical forests across countries between 2000 and 2015. The labels represent the ISO country codes, the position of each label or the grey stick pointing to its estimated hunting pressure and change. A positive change indicates an increase in hunting pressure between 2000 and 2015.

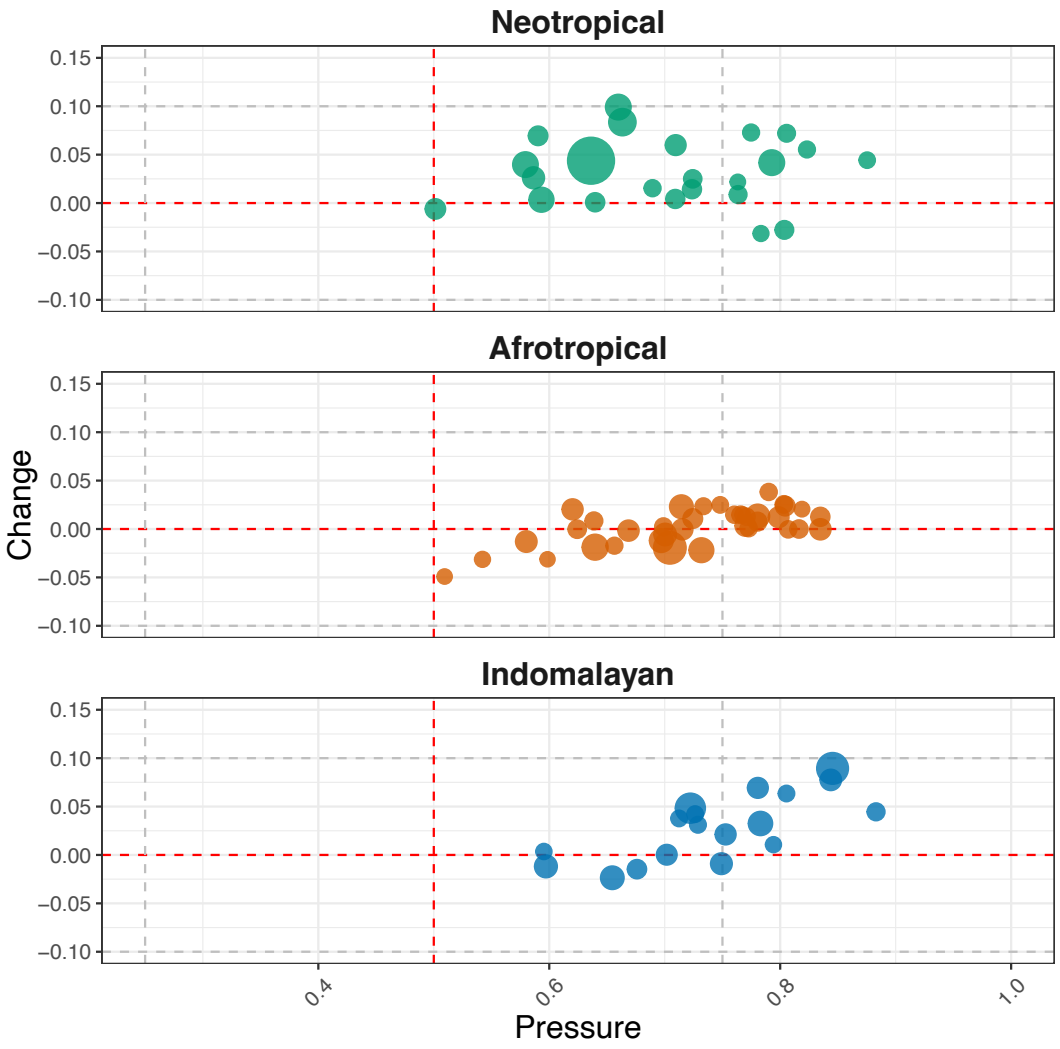

Figure S11. Spatio-temporal variation in predicted hunting pressure in tropical forests across countries between 2000 and 2015. Each country is represented as a point, where point size is proportional to the proportion of the country where hunting could occur. The x-axis represents predicted hunting pressure in 2015, and the y-axis represents change in pressure between 2000 and 2015. Red dashed lines indicate reference thresholds: a pressure value of 0.5 and no change (i.e., change = 0). A positive change indicates an increase in hunting pressure between 2000 and 2015.

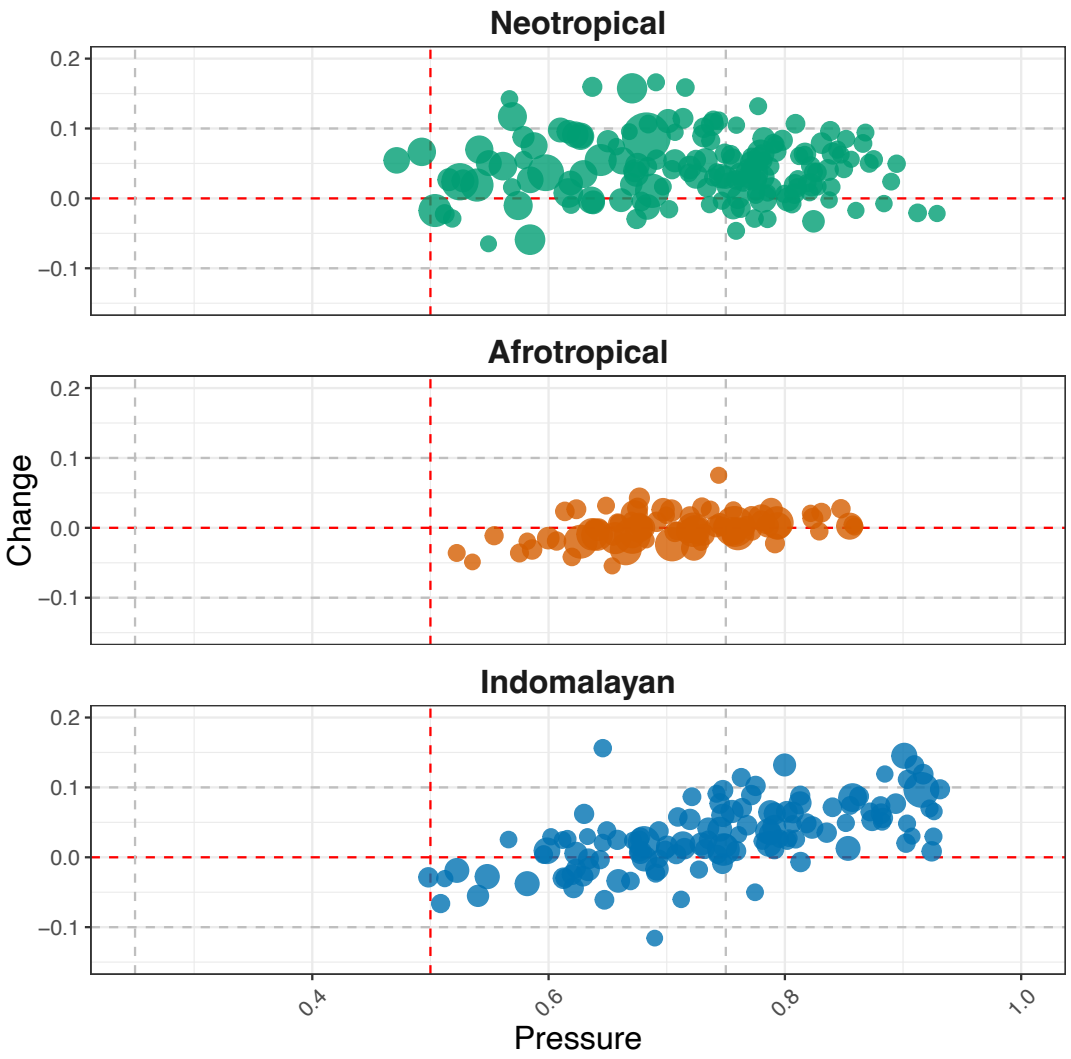

Figure S12. Spatio-temporal variation in predicted hunting pressure in tropical forests across ecoregions between 2000 and 2015. Each ecoregion is represented by a point where point size is proportional to the proportion of the country where hunting could occur. The x-axis represents predicted hunting pressure in 2015, and the y-axis represents change in pressure between 2000 and 2015. Red dashed lines indicate reference thresholds: a pressure value of 0.5 and no change (i.e., change = 0). A positive change indicates an increase in hunting pressure between 2000 and 2015.

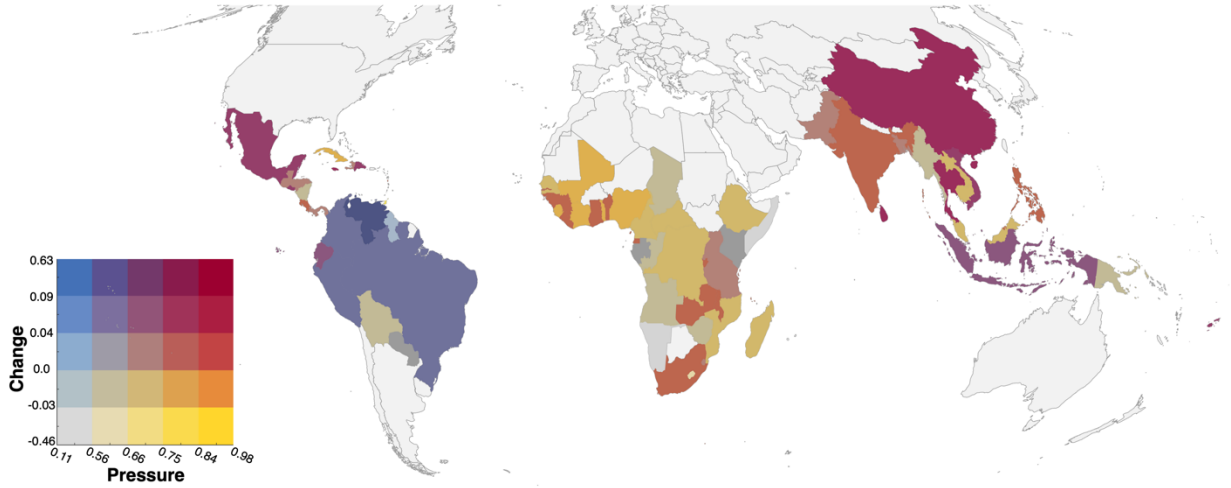

Figure S13. Spatio-temporal variation in predicted hunting pressure in tropical forests across countries between 2000 and 2015. Hunting pressure was predicted at a 1 km × 1 km resolution using spatially explicit environmental and socio-economic predictors from 2000 and 2015 (or the closest available years). Predictions correspond to the median values from 10 independently trained and fine-tuned random forest models, calibrated using random k-fold cross-validation and downsampling to correct for class imbalance (hunted vs. non-hunted sites). The pressure values represent predicted hunting pressure in 2015, while change values indicate the difference between 2015 and 2000 predictions, where negative values reflect a decrease and positive values an increase in pressure over time. Both metrics are categorized by percentiles (0–20%, 20–40%, 40–60%, 60–80%, 80–100%). Pressure and change were then aggregated by country to provide a mean value of pressure and change per country. Combinations of pressure and change percentiles are color-coded as grey: low pressure and decreasing pressure, yellow: high pressure and decreasing pressure, blue: low pressure and increasing pressure or purple: high pressure and increasing pressure.

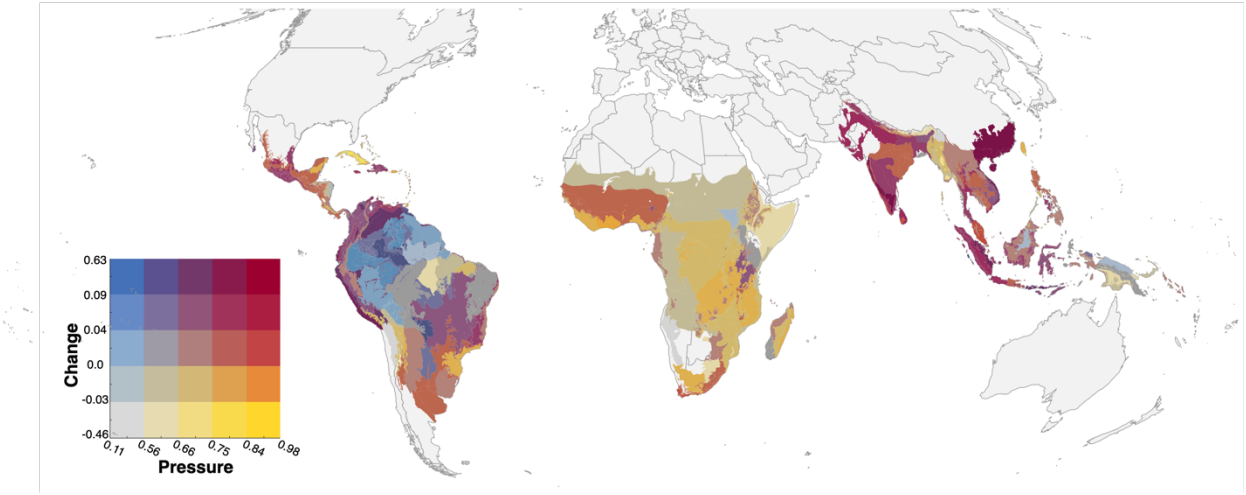

Figure S14. Spatio-temporal variation in predicted hunting pressure in tropical forests across ecoregions between 2000 and 2015. Hunting pressure was predicted at a 1 km × 1 km resolution using spatially explicit environmental and socio-economic predictors from 2000 and 2015 (or the closest available years). Predictions correspond to the median values from 10 independently trained and fine-tuned random forest models, calibrated using random k-fold cross-validation and downsampling to correct for class imbalance (hunted vs. non-hunted sites). The pressure values represent predicted hunting pressure in 2015, while change values indicate the difference between 2015 and 2000 predictions, where negative values reflect a decrease and positive values an increase in pressure over time. Both metrics are categorized by percentiles (0–20%, 20–40%, 40–60%, 60–80%, 80–100%). Pressure and change were then aggregated by ecoregion to provide a mean value of pressure and change per ecoregion. Combinations of pressure and change percentiles are color-coded as grey: low pressure and decreasing pressure, yellow: high pressure and decreasing pressure, blue: low pressure and increasing pressure or purple: high pressure and increasing pressure.

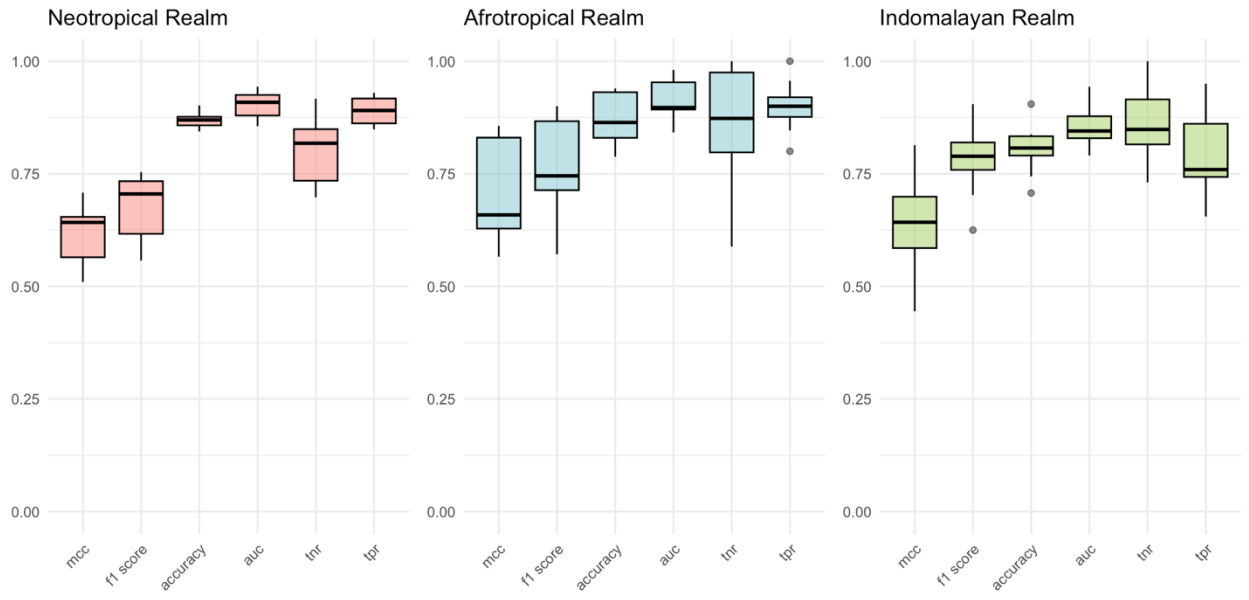

Figure S15. Comparison of goodness-of-fit metrics between supervised learning models fine-tuned and trained independently for each realm. All approaches use random k-fold cross-validation and downsampling to address class imbalance.

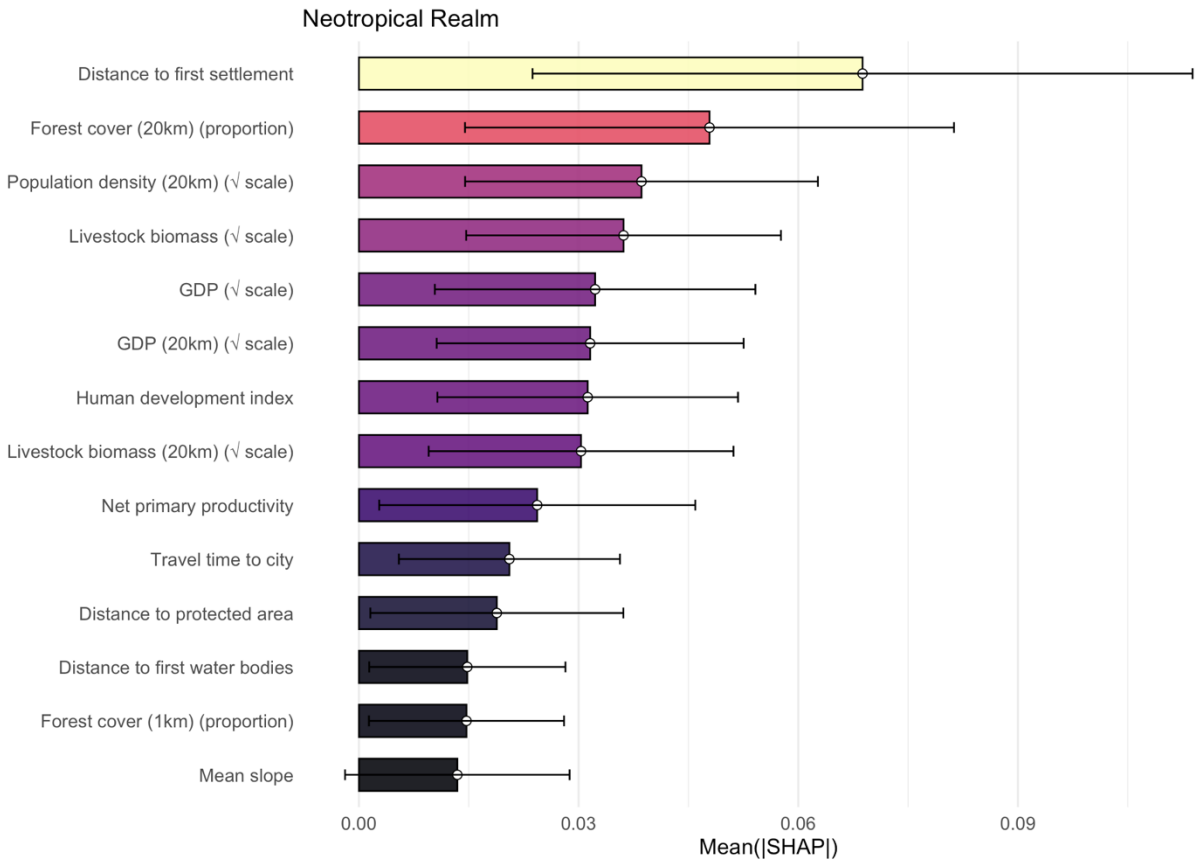

Figure S16. Global importance of ecological and socio-economic predictors in 10 random forest models for the Neotropics. Mean absolute SHAP values are displayed to summarize the overall importance of each predictor across models. The brackets represent the standard deviation and the white dot the mean.

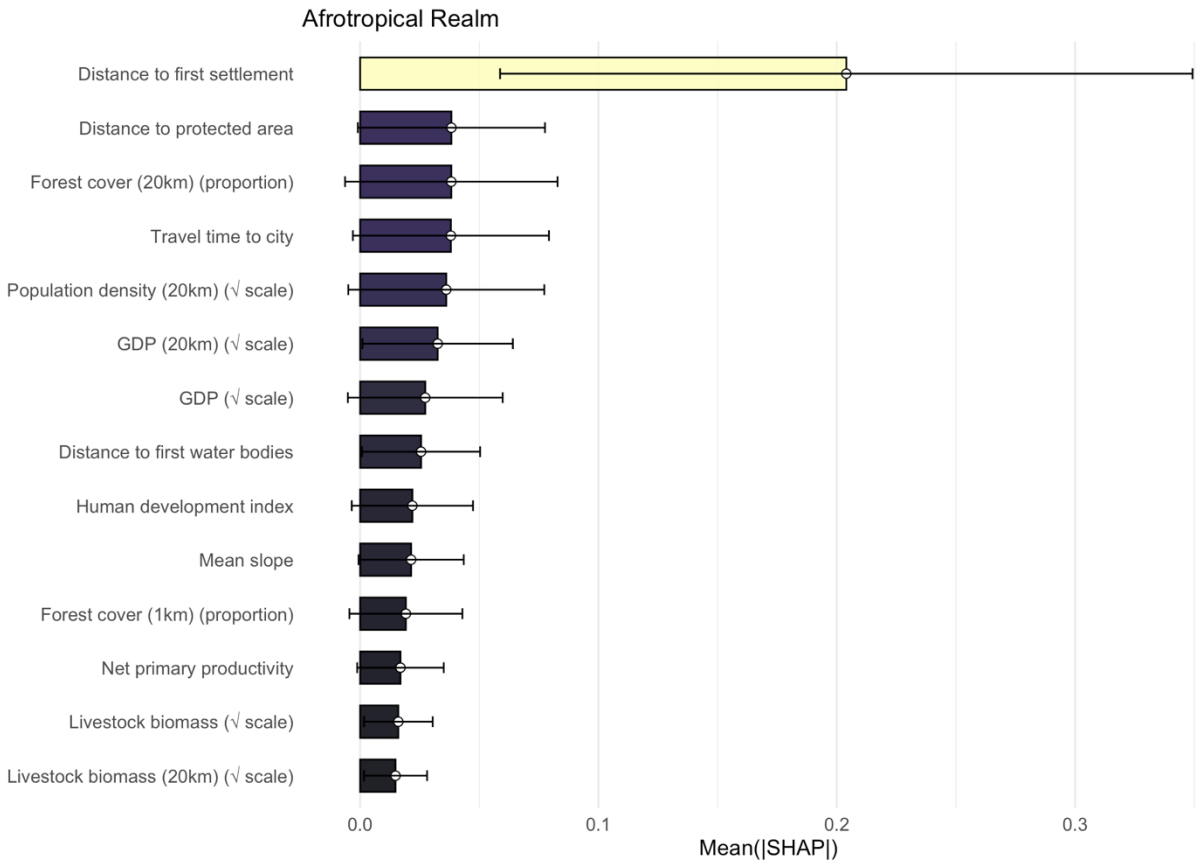

Figure S17. Global importance of ecological and socio-economic predictors in 10 random forest models for the Afrotropics. Mean absolute SHAP values are displayed to summarize the overall importance of each predictor across models. The brackets represent the standard deviation and the white dot the mean.

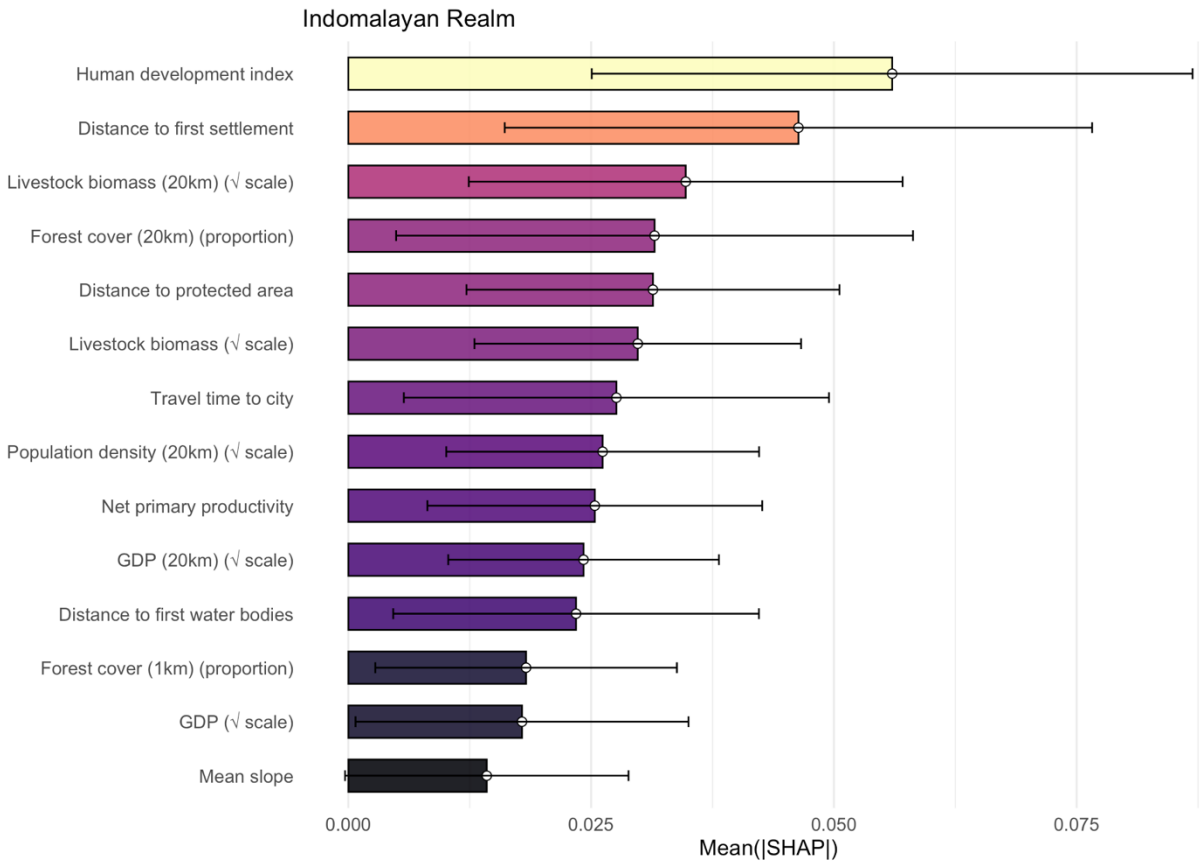

Figure S18. Global importance of ecological and socio-economic predictors in 10 random forest models for the Indomalayan realm. Mean absolute SHAP values are displayed to summarize the overall importance of each predictor across models. The brackets represent the standard deviation and the white dot the mean.

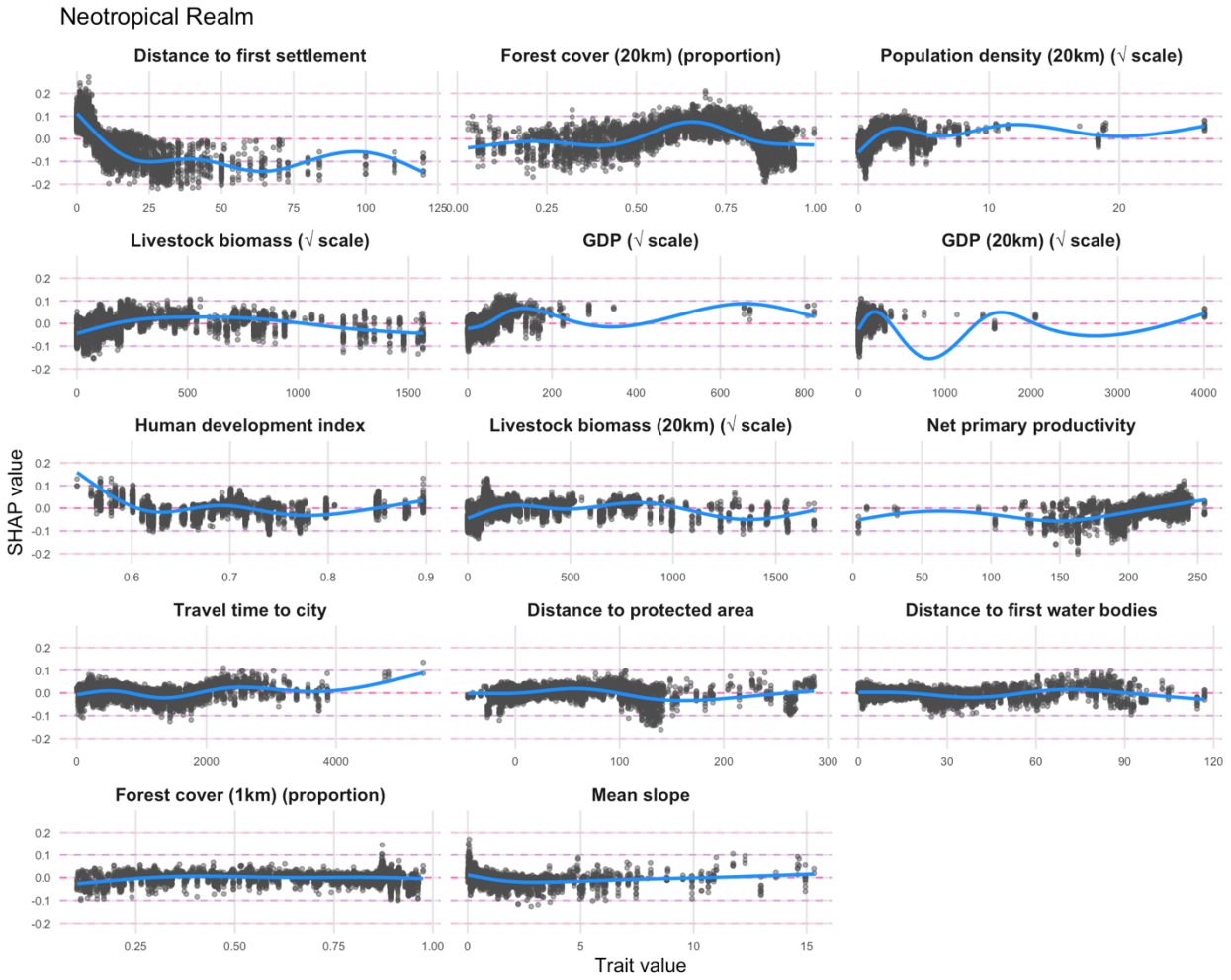

Figure S19. Marginal effects of ecological and socio-economic predictors in 10 random forest models using downsampling for the Neotropics. SHAP values were used to assess the importance of each predictor on the predicted probability of a site being classified as hunted (i.e., hunting pressure). Each point represents a prediction for an individual site in the Neotropics, based on ecological and socio-economic predictors, using the previously trained random forest classifiers. Positive SHAP values indicate that a given predictor increases the likelihood of a site being classified as hunted, while negative SHAP values suggest an association with non-hunted status. A non-linear regression line is included to visualize the shape of each predictor's influence. Additionally, mean absolute SHAP values are displayed to summarize the overall importance of each predictor across models.

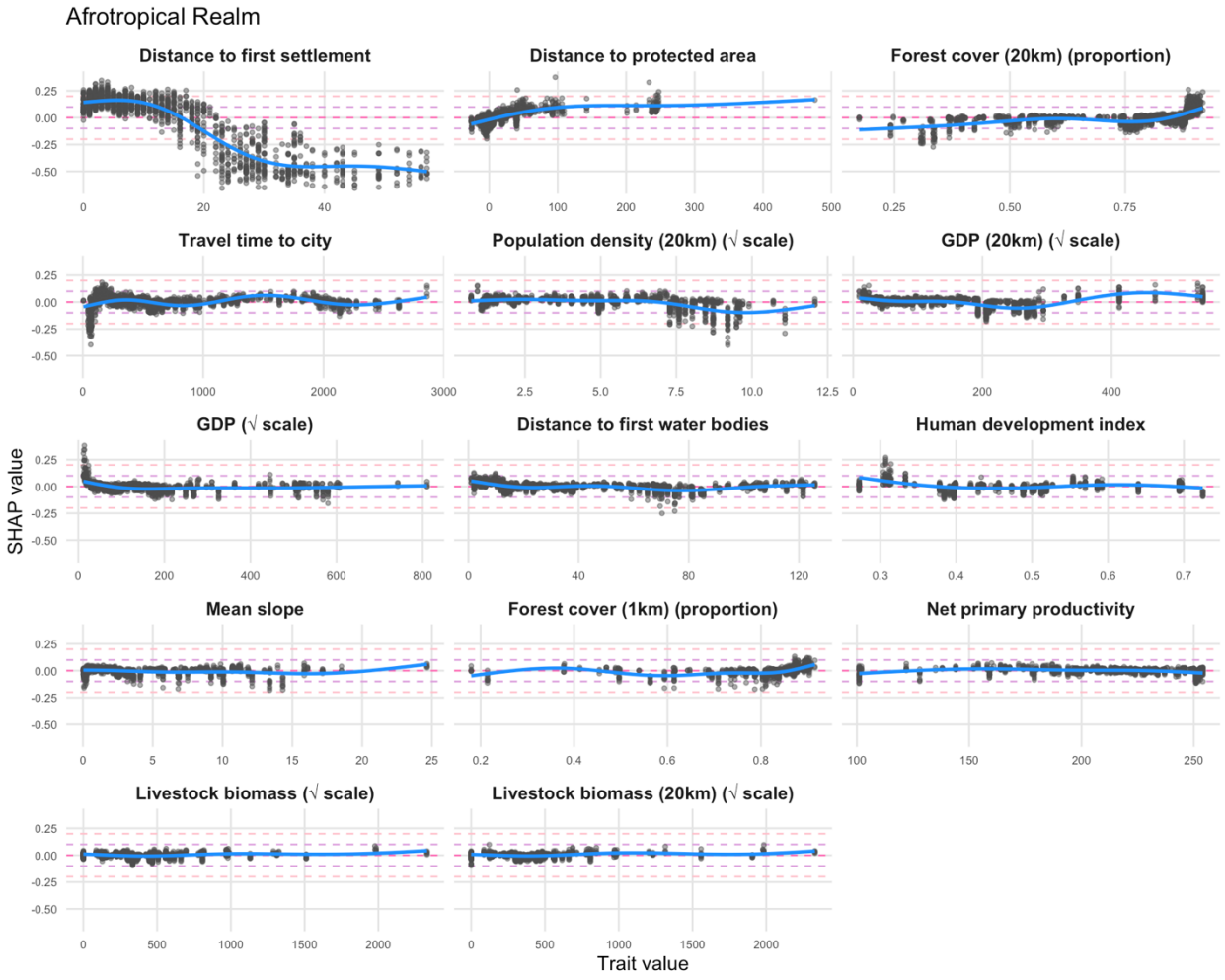

Figure S20. Marginal effects of ecological and socio-economic predictors in 10 random forest models using downsampling for the Afrotropics. SHAP values were used to assess the importance of each predictor on the predicted probability of a site being classified as hunted (i.e., hunting pressure). Each point represents a prediction for an individual site in the Afrotropics, based on ecological and socio-economic predictors, using the previously trained random forest classifiers. Positive SHAP values indicate that a given predictor increases the likelihood of a site being classified as hunted, while negative SHAP values suggest an association with non-hunted status. A non-linear regression line is included to visualize the shape of each predictor's influence. Additionally, mean absolute SHAP values are displayed to summarize the overall importance of each predictor across models.

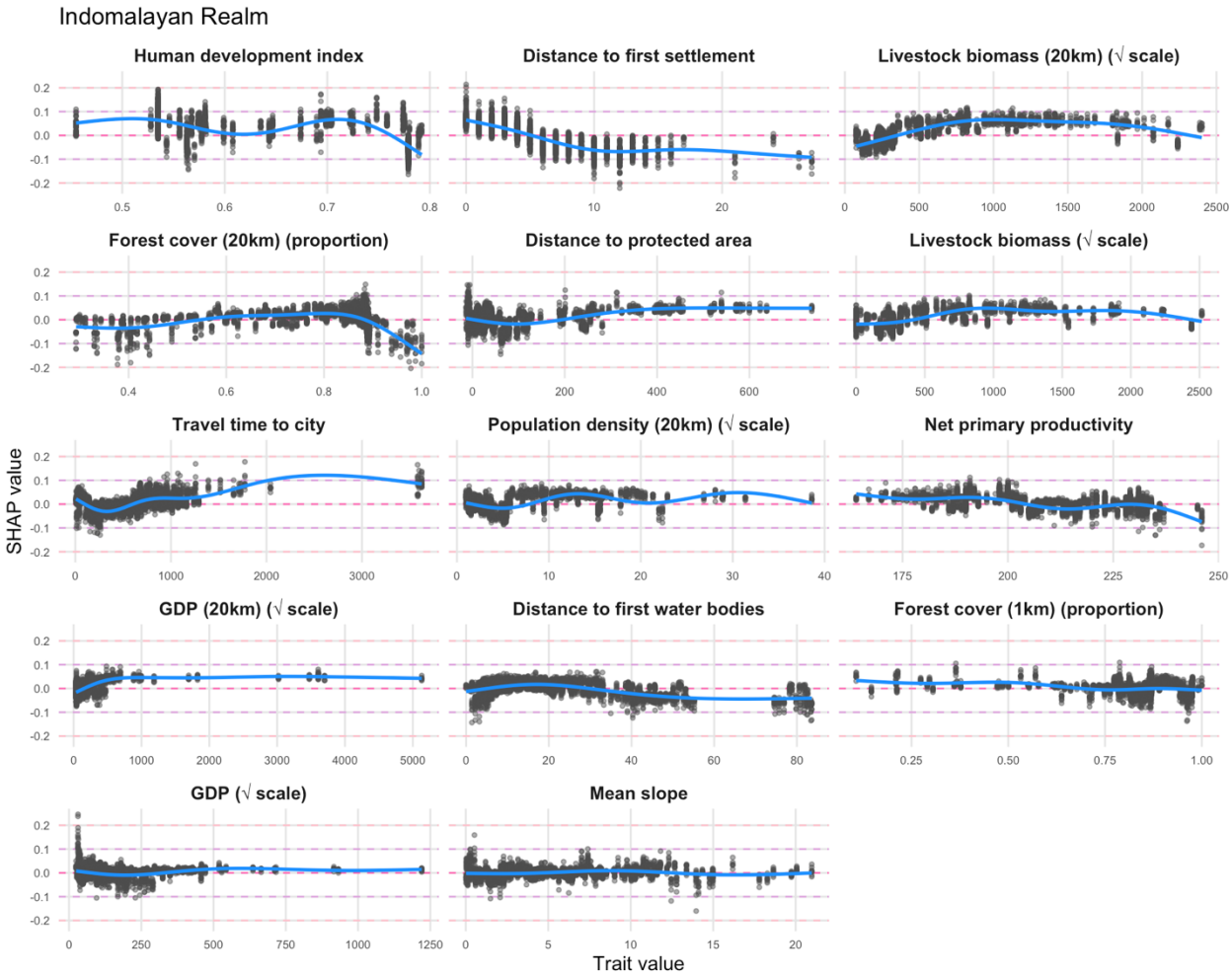

Figure S21. Marginal effects of ecological and socio-economic predictors in 10 random forest models using downsampling for the Indomalayan realm. SHAP values were used to assess the importance of each predictor on the predicted probability of a site being classified as hunted (i.e., hunting pressure). Each point represents a prediction for an individual site in the Indomalayan realm, based on ecological and socio-economic predictors, using the previously trained random forest classifiers. Positive SHAP values indicate that a given predictor increases the likelihood of a site being classified as hunted, while negative SHAP values suggest an association with non-hunted status. A non-linear regression line is included to visualize the shape of each predictor's influence. Additionally, mean absolute SHAP values are displayed to summarize the overall importance of each predictor across models

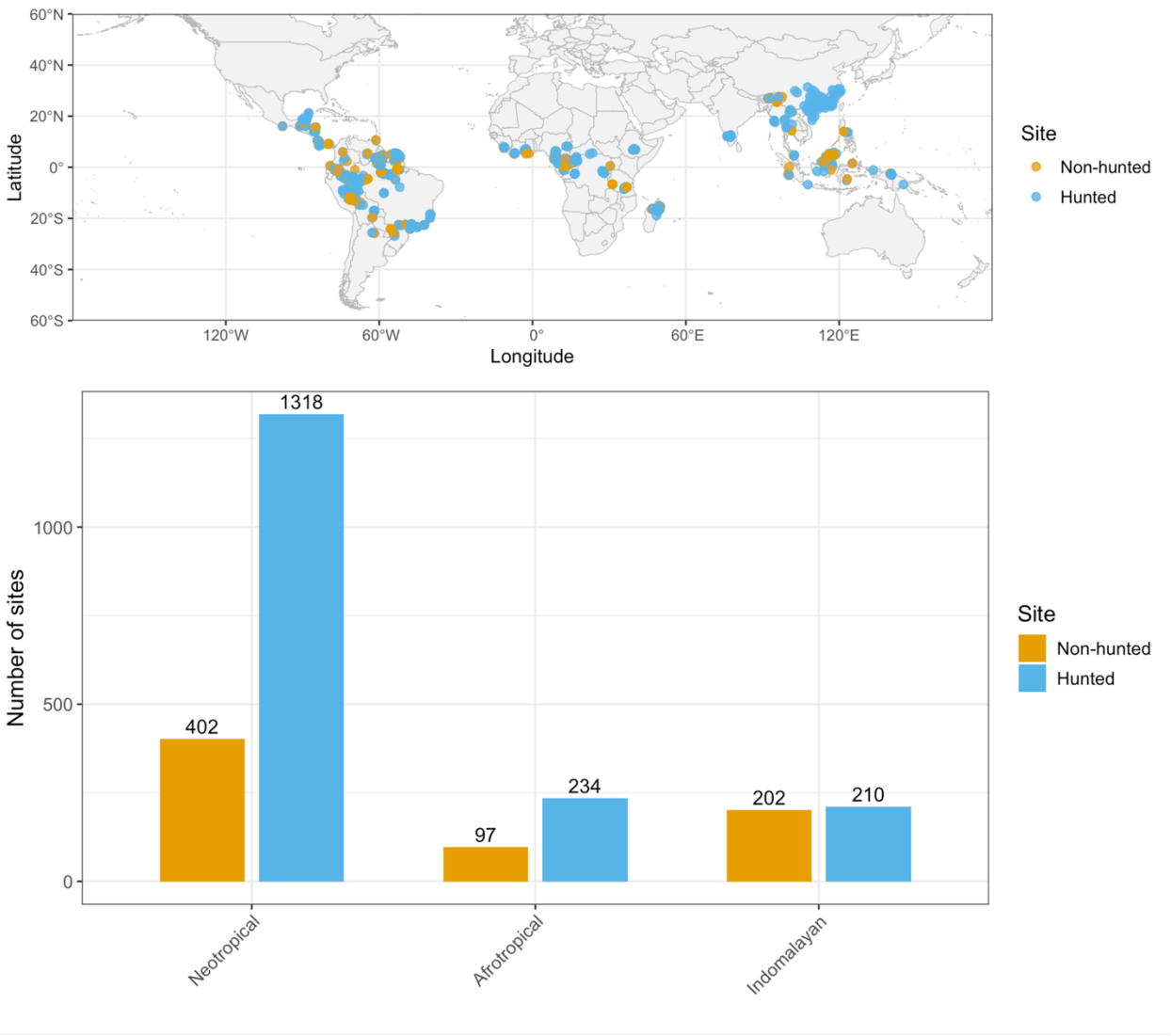

Figure S22. Geographic distribution of study sites and their hunting status across tropical forests. Map showing the spatial distribution of all study sites used in the analysis across the tropical biome, color-coded by hunting status. Each point represents a site classified as either hunted or non-hunted. This distribution highlights spatial coverage across the Neotropical, Afrotropical and Indomalayan realms and the imbalance in sample representation between hunted and non-hunted sites.

Supplementary Reference

Copernicus Climate Change Service, Climate Data Store, (2019): Land cover classification gridded maps from 1992 to present derived from satellite observation. Copernicus Climate Change Service (C3S) Climate Data Store (CDS). DOI: 10.24381/cds.006f2c9a

Liaw A, Wiener M (2002). "Classification and Regression by randomForest." *R News*, **2**(3), 18-22. https://CRAN.R-project.org/doc/Rnews/.

Mattia Marconcini, Annekatrin Metz-Marconcini, Thomas Esch and Noel Gorelick. Understanding Current Trends in Global Urbanisation - The World Settlement Footprint Suite. GI_Forum 2021, Issue 1, 33-38 (2021). https://austriaca.at/0xc1aa5576%200x003c9b4c.pdf

Pebesma, E. (2018). Simple features for R: standardized support for spatial vector data.

Weiss, D. J., Nelson, A., Gibson, H. S., Temperley, W., Peedell, S., Lieber, A., Hancher, M., Poyart, E., Belchior, S., Fullman, N., Mappin, B., Dalrymple, U., Rozier, J., Lucas, T. C. D., Howes, R. E., Tusting, L. S., Kang, S. Y., Cameron, E., Bisanzio, D., ... Gething, P. W. (2018). A global map of travel time to cities to assess inequalities in accessibility in 2015. *Nature*, *553*(7688), 333–336.

Wright, M. N., & Ziegler, A. (2015). ranger: A fast implementation of random forests for high dimensional data in C++ and R. *arXiv preprint arXiv:1508.04409*.